Biochimica et Biophysica Acta 1838 (2014) 398–412

Contents lists available at ScienceDirect

Biochimica et Biophysica Acta

journal homepage: www.elsevier.com/locate/bbamem

PEGylated cationic liposome–DNA complexation in brine is pathway-dependent

Bruno F.B. Silva [a,b,c,d,*], Ramsey N. Majzoub [a,b,c], Chia-Ling Chan [a,b,c,e,f], Youli Li [g], Ulf Olsson [d], Cyrus R. Safinya [a,b,c,**]

[a] Department of Materials, University of California, Santa Barbara, CA 93106, USA
[b] Department of Physics, University of California, Santa Barbara, CA 93106, USA
[c] Molecular, Cellular & Developmental Biology Department, University of California, Santa Barbara, CA 93106, USA
[d] Division of Physical Chemistry, Centre for Chemistry and Chemical Engineering, Lund University, P.O. Box 124, SE-221 00 Lund, Sweden
[e] Institute of Physics Academia Sinica, Taipei 11529, Taiwan
[f] National Synchrotron Radiation Research Center, Hsinchu 30076, Taiwan
[g] Materials Research Laboratory, University of California, Santa Barbara, CA 93106, USA

ARTICLE INFO

Article history:
Received 7 June 2013
Received in revised form 20 August 2013
Accepted 11 September 2013
Available online 20 September 2013

Keywords:
CL–DNA
Lipoplex
Salt
Steric stabilization
SAXS
Gene therapy

ABSTRACT

Cationic liposome–DNA (CL–DNA) complexes, are regarded as promising materials for safe and efficient delivery of genes for therapeutical applications. In order to be used in vivo, these complexes may be coated with a hydrophilic polymer (e.g. polyethylene-glycol, PEG) that provides steric stabilization towards adhesion of proteins and removal by the immune system. In this work we study the influence of the initial salt concentration (C_s) – which modulates the electrostatic interaction between oppositely charged vesicles and DNA – on the structure and stability of PEGylated CL–DNA particles. Previous small-angle X-ray scattering has shown that if non-PEGylated or PEGylated CL–DNA lamellar complexes are prepared in water, their structure is well defined with a high number of lipid membrane–DNA layers (larger than 20). Here we show that if these complexes are transferred to saline media (150 mM NaCl or DMEM, both near physiological conditions), this structure remains nearly unchanged. Conversely, if PEGylated complexes are prepared in saline media, their lamellar structure is much looser, with fewer number of layers. This pathway dependent behavior of PEGylated complex formation in brine is modulated by the liposome membrane charge density and the mole fraction of PEG 2000 in the membranes, with the average number of layers decreasing with increasing C_s and in going from 5 mol% to 10 mol% PEG-lipid. Each of these structures (high and low number of layers) is stable with time, suggesting that despite complex formation being thermodynamically favored, the complexation process in PEGylated membranes, which determines the number of layers per particle, is kinetically controlled. In the extreme case (when polymer repulsions from 10 mol% PEG-lipid are maximized and electrostatic attraction between PEGylated CLs and DNA are minimized at low membrane charge density) complex formation is suppressed at high $C_s = 150$ mM.

1. Introduction

Cationic lipid–DNA complexes (commonly abbreviated to CL–DNA or lipoplexes) hold great promise as efficient and safe synthetic gene vectors for gene therapy applications [1–5]. Some of the most attractive advantages include: reduced immune response, virtually no limit on the size of carried DNA, and potential for large-scale production, among others. However, much remains to be learned about the interactions of lipoplexes with biological systems (i.e. cells, tissues, organs), and how to tailor their structure and function, in order to successfully overcome all the barriers, from particle synthesis to gene delivery inside targeted cell nuclei [1,2,4–6].

CL–DNA complexes can be found in four main morphologies: lamellar (L_α^C), where DNA rods are sandwiched between lipid bilayers [7,8]; inverse hexagonal (H_{II}^C), where DNA rods are enclosed in rod-like inverted micelles organized in a hexagonal lattice [9]; normal hexagonal (H_I^C), where rod-like lipid micelles arranged on a hexagonal lattice have DNA inserted within the interstices in a honeycomb-like pattern [10]; and distorted H_I^C phases with multivalent lipids [11]. The main parameters controlling the resulting structure are (i) the spontaneous curvature of the lipid and (ii) membrane flexibility [9]. Cubic phases in lipid–Nucleic acid systems have been reported with short RNA [12,13], and in rare cases for long DNA [14].

* Correspondence to: B.F.B. Silva, Division of Physical Chemistry, Centre for Chemistry and Chemical Engineering, Lund University, P.O. Box 124, SE-221 00 Lund, Sweden. Tel.: +46 72 394 22 44; fax: +46 46 222 44 13.
** Correspondence to: C.R. Safinya, Department of Materials, University of California, Santa Barbara, CA 93106, USA. Tel.: +1 805 893 8635; fax: +1 805 893 8797.
E-mail addresses: brunobrasdasilva@gmail.com (B.F.B. Silva), safinya@mrl.ucsb.edu (C.R. Safinya).

0005-2736/$ – see front matter © 2013 Elsevier B.V. All rights reserved.
http://dx.doi.org/10.1016/j.bbamem.2013.09.008

It has been found that each of these structures interacts with cells via different mechanisms, giving rise to different transfection efficiencies. Particularly striking was the finding that transfection efficiency (TE) in overall positively charged L_α^C complexes has a bell-shaped dependency on the complex's membrane charge density (σ_M) [15,16]. Despite all of this progress, when CL–DNA complexes are administrated in vivo, the TE is still very low. A major contributing factor to low TE seems to come from the coating of lipoplexes by blood proteins which may render them inactive (e.g. by changing the zeta potential from positive to negative), destabilize them [17], or lead to active removal by the immune system [18]. This problem is not restricted to CL–DNA particles, but common to most non-viral particle drug-delivery systems administered through blood [19–21].

It becomes therefore necessary to protect CL–DNA particles, or in the more general case, liposomes, from protein adsorption and removal by immune cells. Given the coexistence of phagocytes with red blood cells (erythrocytes) in the blood stream, the first strategy was the preparation of liposomes mimicking the red cell membranes. The liposome surface was therefore modified with the sterically hindered ganglioside GM_1 or phosphatidylinositol (PI), which led to a significant enhancement in the circulation time of the now-called "stealth" or "sterically stabilized" liposomes [22–24]. After these first successful attempts, it was realized that other flexible-chained hydrophilic polymers were also successful at increasing the circulation time of liposomes in blood. In particular, the use of polyethylene glycol (PEG)-lipids, with PEG $M_r = 1900$ or 5000 provided longer circulation times compared to GM_1 and PI [25–30], which when combined with the ease of use and availability of these synthetic polymers, led to the use of PEG-lipids as the prime choice for stealth liposomes [19]. As suggested [19,20,31], when the PEG chains at the surface of the liposome are approached by colloidal objects, they become confined, leading to a reduction of the entropy of the polymer chain. This produces a repulsive force, which prevents the attachment of blood opsonins and other elements.

It has been shown that cationic lipid membranes incorporating PEG2K-lipids successfully associate with DNA leading to the formation of PEG–CL–DNA particles with L_α^C structure [32]. It has been also shown that complexes incorporating PEG have endured colloidal stability, and their TE dropped by orders of magnitude, indicating that the polymer coat is indeed providing steric stabilization against aggregation, but also against fusion of the CL–DNA with the endosomal membranes in cells, in what has been described as the "PEG dilemma" [5,33]. Some ongoing research is now aiming at recovering the TE in PEGylated particles. The use of diffusible PEG conjugates [34,35], where a smaller hydrophobic moiety allows the PEG lipid to leave the complexes after some time, or cleavable PEG-lipids [33,35,36], where the PEG chain can be detached by the hydrophobic moiety by a change in pH, redox potential, or by the action of an enzyme, has proven to considerably improve the TE. The development of new cationic moieties, like multivalent headgroups [11] or pH-sensitive ionizable lipids [37], and peptide signals for directed cell–receptor interactions [38], among others, also provide improved TE in many instances. All of these functionalities may be advantageous for certain applications, and clearly, future safe and efficient gene vectors will need to incorporate multiple functions to overcome both extracellular and intracellular barriers [5].

The main driving force for complex formation comes from the high entropic gain achieved by counterion release when both components (cationic lipid and DNA) neutralize each other [7,39–41]. Thus, while CL–DNA formation is sensitive to the concentration of ions in the preparation media, it was found out that for physiological conditions (monovalent salt concentration $\approx$ 150 mM), salt effects are not very significant [42]. However, the incorporation of PEG2K-lipids in cationic liposomes, which stabilizes liposomes against aggregation from blood proteins due to the aforementioned repulsive force from PEG2K, also opposes complexation with DNA. This is because the PEG2K polymer becomes confined to the water pockets between the lipid membranes and DNA in complexes, which leads to a loss of entropy of the polymer chain [31]. The interplay between electrostatic effects, that favor complexation and are salt dependent, and PEG2K repulsion, that opposes complexation, should then lead to interesting effects, when producing sterically-stabilized lipoplexes. We should note that while previous work has shown that PEG2K–CL–DNA complexes can form well defined particles in water, and have been used in TE and live cell imaging experiments where they are prepared in culture media (with monovalent salt concentration near physiological conditions — 150 mM) [32], a detailed characterization of the salt effect on the structure and stability of these complexes is still lacking.

One of the goals of this work is then to study the influence of both of these colloidal forces: steric repulsion (modulated by PEG surface coverage) and electrostatic attraction (modulated by membrane charge density (σ_M) and salt concentration (C_s)) on the structure and stability of PEGylated complexes. Simultaneously, and perhaps more importantly, we aim also at an understanding of whether the order of mixing of these three components (CL, DNA and salt) is relevant or not, i.e. if the structure of PEGylated and non-PEGylated lipoplexes is pathway dependent and thus different whether they are prepared in water and transferred to saline media later, or prepared in saline media from the very beginning. This second aspect is important since both methods of preparation can be found in the literature, but with the differences not being addressed or discussed (see e.g. Refs [18,42] and the protocol for Lipofectamine® 2000 [43]).

As will be seen further below, the final structure of PEGylated complexes, namely the amount of lipid-DNA layers per particle, is found to depend to a large extent on whether salt is added before, or after complex formation. This effect, by itself, is likely to affect the overall TE of CL–DNA particles, but perhaps more importantly, it has the potential to be used as a means to further manipulate and tailor the final structure of CL–DNA particles, designed to perform different functions.

In the more general case, this interplay between colloidal forces of opposite sign, and the ease in which one can control them (e.g. PEG chain length and grafting density for modulating the steric repulsion; membrane charge density and salt ionic strength for modulating the electrostatic attraction) can provide a suitable way to manipulate colloidal interactions as a means to control the phase behavior of a number of systems and tailor the structure of different types of particles. Controlling interparticle interactions and aggregation is of central importance in a number of areas, ranging from cluster formation in various disease processes to rheological control in food products and lubricants.

2. Materials and methods

The lipids 1,2-dioleoyl-*sn*-glycero-3-phosphocholine — DOPC; 1,2-dioleoyl-3-trimethylammonium-propane (chloride salt) — DOTAP; and 1,2-dioleoyl-*sn*-glycero-3-phosphoethanolamine-N-[methoxy(polyethylene glycol)-2000] (ammonium salt) — 18:1 PEG2000 PE solubilized in chloroform were purchased from Avanti Polar Lipids and used as received. These lipids, which are easily obtained, are good model systems for more complicated custom-designed molecules, and therefore, the main conclusions from this study should be extendable to more complicated formulations including PEG-lipids. Two parameters are systematically changed in the lipid composition (Table 1): (i) the lipid membrane charge density (σ_M), which is proportional to the amount of DOTAP molar fraction in the membrane; and (ii) the amount of PEG2K lipid (0, 5 and 10% molar fraction). The lipids are mixed in chloroform in the appropriate ratios and final concentration (30 mM for the SAXS samples and 2 mM for the colocalization samples). For the colocalization experiments, Texas-Red lipid in chloroform (1 mg/ml) is added in a 0.2%(mol/mol) ratio to the total lipid. The resulting mixture was dried first under a constant stream of nitrogen for 5 min, and then in vacuum for approximately 24 h to get rid of

any residual amount of chloroform. Ultra-pure (Milli-Q) water is then added to the dry lipid film to obtain a final concentration of 30 mM (DOTAP + DOPC + PEG2000) for the SAXS experiments, and 2 mM for the colocalization. The resulting mixture is incubated at 37 °C for an additional 24-hour period. This ensures that the whole lipid film has been hydrated. The mixture is then sonicated for 7 min at 40 MHz, resulting in a uniform suspension of liposomes with ca., 50 nm radius. The samples are then kept at 4 °C, where they are stable for several days. If signs of aggregation are noticed (e.g. if turbidity increases), the samples are sonicated again before usage.

Calf thymus DNA (Sigma) with a hydration of ca. 25% is weighed in a vessel and the desired amount of water is added. The vessel is very gently mixed (no vortex) to avoid breakage of the DNA chains, and incubated at 37 °C. For the colocalization experiments, YOYO-1 1 mM solution in DMSO (Molecular Probes) is added in a ratio 1:26 base pairs before incubation. After 24 h the mixture is homogeneous and the DNA concentration is determined with a NanoDrop spectrometer before storage at 4 °C. For X-ray samples, the used DNA concentration was ca. 3 mg/ml. For the colocalization samples, the DNA concentration was ca. 0.12 mg/ml.

In addition to the membrane charge density (σ_M) and amount of PEG2K (Table 1), an additional composition parameter in the complexes is the charge ratio ρ, which is the ratio of cationic to anionic charges ($\rho = n_{DOTAP}/2n_{DNAbp}$, where n_{DOTAP} and n_{DNAbp} stand for mole of DOTAP and DNA base pairs in the sample, respectively). For $\rho = 0.5$, the complexes are overall negatively charged, and there is excess of free DNA in the solution. For $\rho = 1$ the complexes are practically neutral. For $\rho = 3$ the complexes are overall positively charged and there is excess of free liposome in the solution. TE studies in the past have shown that only positively charged complexes are able to transfect. One of the most efficient charge ratios is $\rho = 10$, and for that reason, this ratio is also studied in this work.

2.1. Complex preparation

Two preparation methods are studied in this work. In the first, the complexes are prepared in water, and transferred later to saline media. This method will be nicknamed “After”. In the second, when cationic lipid and DNA are mixed, they are already in saline media. This method will be nicknamed “Before”. The salt compositions 50, 100 and 150 mM NaCl were studied. In addition, we studied also DMEM (Dulbecco's Modified Eagle Medium), since it is a common preparation media used in several TE studies, with ionic strength close to physiological conditions (≈150 mM monovalent salt). Regardless of the preparation methods, the amount of DNA in SAXS samples is fixed to 25 μg for $\rho > 0.5$, and 50 μg for $\rho = 0.5$. For colocalization samples, the amount of DNA is fixed to 0.5 μg and $\rho = 5$. The amount of lipid is added according to ρ.

After: for the SAXS measurements, lipid and DNA are added to an Eppendorf tube, and centrifuged for 10 min at 21 000 rpm. If a pellet has not been formed, the tube is vortexed for ca. 5 s, and centrifuged for 30 min more. The tube is put at 4 °C for ca. 24 h, and after, the required volume of a NaCl 300 mM solution is added to adjust to the final desired salt concentration. In the case of DMEM, we added a volume of 1.5 ml to the pellets, so that the volume of the CL–DNA pellet plus supernatant has a small dilution effect on the DMEM composition. After 2 days at 4 °C, the pellets are transferred to quartz X-ray capillaries (Hilgenberg), which are subsequently flame sealed to avoid solvent losses. The samples are, as much as possible, kept at 4 °C, except for ca. 12 h before the measurements. For the colocalization experiments, the vesicles and DNA are mixed ($\rho = 5$) and gently homogenized. An equal volume of 300 mM NaCl is added after 24 h, to bring the total salt concentration to 150 mM. Colocalization measurements were performed 30 min and 24 h after salt addition.

Before: The process is identical to the previous, with the difference that DNA is transferred to an Eppendorf tube, and the required volume of a NaCl 300 mM solution is added. The Eppendorf tube is homogenized, and subsequently the calculated volume of cationic lipid is added to the DNA in salt. (We also tested with both lipid and DNA already in salt, and the results are identical). In this way, DNA and lipid mix already under saline conditions. For the colocalization experiments, DNA is added to a 300 mM NaCl solution (the volume is set in such a way that when adding the liposome solution, the total salt concentration is 150 mM). The sample is gently homogenized, and the corresponding volume of vesicles is added after. The sample is again gently homogenized. Colocalization measurements were performed 30 min and 24 h after the liposome addition.

2.2. Colocalization

For fluorescence colocalization studies, samples were prepared by applying 2 μl of CL–DNA complex containing solution between a glass slide and coverslip which was sealed using vacuum grease. Images were acquired at the NRI-MCDB Microscopy Facility at UC-Santa Barbara. The imaging system is an Olympus DSU equipped with a LUCPLanFLN 40× objective. YOYO-1 dye was visualized using a 89000 Sedat Quad Filter with excitation/emission of 490/525 nm while the Texas-Red dye was visualized using a Semrock Pinkel Filter with em/ex of 589/639 nm. Images were captured using a Hamamatsu ImagEM CCD Camera (C9100-13) where both camera and microscope are controlled via Metamorph software.

2.3. Small-angle X-ray scattering (SAXS)

Small-angle X-ray diffraction was performed at beamline 4–2 of the Stanford Synchrotron Radiation Lightsource (SSRL) and in our in-house device. At the SSRL, the data was collected in different runs. The used X-ray wavelength (λ) was either 1.24 or 1.1 Å, and the sample to detector distance was either 0.5 or 1.2 m. Data were collected on a MX-225 Rayonix CCD detector. The resolution of the instrument (full-width-at-half-maximum — FWHM) was estimated from the geometry of the instrument, and is $\approx 1.3–1.8 \times 10^{-3}$ Å^{-1} (depending on the exact configuration). The in-house instrument uses a fixed X-ray generator tube ($\lambda = 1.54$ Å), and a Mar345 detector at a sample-to-detector distance of 1.4 m. Each configuration was calibrated with Silver Behenate, and the data expressed in $I(q)$ vs. scattering vector (q). The obtained 2-D scattering patterns were radially integrated either with Fit2D (ESRF) or SAXSi (Roy Beck) programs, and corrected for background by subtracting the signal of a capillary filled with water.

Most of the samples show a scattering pattern typical of lamellar complexes with DNA monolayers sandwiched between the lipid bilayers [7]. Layered arrangements have Bragg peaks repeating at q_{00l} with $l =$

Table 1
Used lipid compositions. All units are molar %.

% mol/mol	0% PEG2K		5% PEG2K			10% PEG2K		
	DOTAP	DOPC	DOTAP	DOPC	18:1-PEG2K PE	DOTAP	DOPC	18:1-PEG2K PE
High $\sigma_M \approx 11 \times 10^{-3}$ e·Å^{-2}	80	20	80	15	5	80	10	10
Low $\sigma_M \approx 4 \times 10^{-3}$ e·Å^{-2}	30	70	30	65	5	30	60	10

1,2,3…, where the lamellar lattice spacing d ($d = \delta + d_w$, with δ standing for the bilayer and d_w for the water thicknesses) is obtained by $d = 2\pi/q_{001}$. In these L_α^C phases the in-plane periodic arrangement of DNA rods sandwiched between the lipid bilayers also gives rise to a peak of periodic distance $d_{DNA} = 2\pi/q_{DNA}$, and is dependent on σ_M, ρ and PEG2K% [7,32,42]. More structural information is included in the shape of these peaks [44–48], as will be seen below. As a general guideline, narrower peaks imply a more organized structure than broad peaks (e.g. the lamellar arrangement has a higher order than the DNA arrangement). d_w in well structured complexes is 25 Å (the diameter of hydrated DNA).

In three-dimensional (3D) materials where the density is periodically modulated along 1D (e.g. smectic A liquid crystals (LCs) and lyotropic LC multilamellar membranes) true long-range order is destroyed by thermally induced layer displacements that diverge logarithmically with sample size (the well established Landau-Peierls effect [49,50]). Hence, the structure factor of the lamellar phase exhibits power law singularities rather than δ-function Bragg diffraction peaks, characteristic of long-range order. These effects are included in the original calculation of the smectic A structure factor by Caillé [44] and have been demonstrated in thermotropic [46] and lyotropic LC systems [45]. Here, we are also interested in the number of layers (n_L) in complexes and therefore, finite size effects are also incorporated in the theory, as well as a powder average over all orientations [45]. We used the expression from Ref [45] for fits of the SAXS data to the theoretical X-ray intensity:

$$S(q) = \frac{4(2\pi)^2}{q}\int_0^\infty dz\left[\cos(q_{00l}z)\exp\left(-z^2\pi/L^2\right)\right]\int_0^\infty \rho d\rho \times\left[\left(\frac{2a}{\rho}\right)^{2\eta}\exp\left(-\eta_{00l}E_1\left(\rho^2/4\lambda z\right)\right)\frac{\sin\left(q\left(z^2+\rho^2\right)\right)^{1/2}}{\left(z^2+\rho^2\right)^{1/2}}\exp\left(-\rho^2\pi/L^2\right)\right] \quad (1)$$

Here, q and z are reciprocal and real space lengths; q_{00l} is the position of the lamellar peak 00 l; L is the domain size; a is of the order of intermolecular distance; η_{00l} is a fitting parameter, and if smaller than 1, $\eta_{00l} \equiv (l^2 q_{00l} k_B T)/(8\pi(BK)^{0.5})$, with k_B being the Boltzmann constant, T as the absolute temperature, B as the bulk compressional modulus, and K as the bulk bending elasticity; E_1 is the exponential integral; and λ is the penetration length, a fitting parameter, typically ≈10 Å. The domain size L is a central parameter in this work, since it provides the lengths over which the lamellar layers are coherent [45], which in the case of discrete particles directly relates with the particle size, and hence, with the number of layers per particle.

L is also approximately ≈2π/FWHM of the lamellar peak. When L_α^C complexes have large domain sizes, the lamellar peak's FWHM starts decreasing, becoming comparable to the resolution of the instrument. The measured domain size from complexes is then convoluted with the resolution of the instrument. Because both the instrument resolution and Eq. (1) can be both approximated by Gaussian equations, the measured domain size (L) is a sum of both Gaussians, and the corrected domain size (L_T) can be calculated with reasonable accuracy according to

$$\left(\frac{2\pi}{L}\right)^2 = \left(\frac{2\pi}{L_T}\right)^2 + \mathrm{FWHM}^2 \quad (2)$$

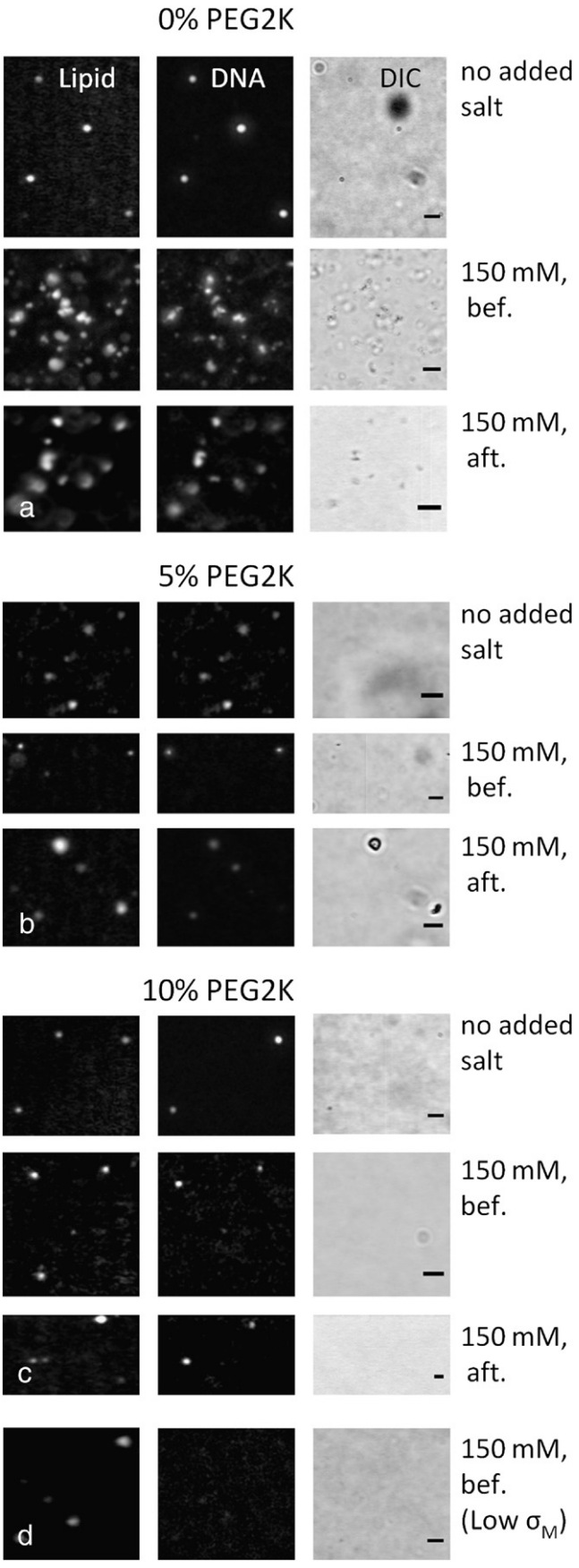

Fig. 1. Colocalization assay with dual fluorescent labeling of CL–DNA complexes allows for simultaneous imaging of lipid (left column) and DNA (middle column). Differential-Interference-Contrast (DIC) micrographs are shown on the right column. (a) High membrane charge density complexes ($\sigma_M \approx 11 \times 10^{-3}$ e·Å^{-2}) without PEG2K (DOTAP/DOPC; 80/20, c.f. Table 1) show strong colocalization when formed in either water or 150 mM NaCl. At high salt concentration, complexes aggregate and form large (>1 μm) aggregates. (b, c) High σ_M complexes containing 5% (DOTAP/DOPC/PEG2K; 80/15/5) or 10% PEG2K (DOTAP/DOPC/PEG2K; 80/10/10) show strong colocalization but remain as diffraction limited objects in salt buffer. (d) At low membrane charge density ($\sigma_M \approx 4 \times 10^{-3}$ e·Å^{-2}) and 10% PEG2K (DOTAP/DOPC/PEG2K; 30/60/10), complexes formed in 150 mM NaCl show reduced colocalization. All scale bars (lower right corner of DIC micrographs) are 5 μm.

where FWHM is the resolution of the instrument. The number of layers (n_L) per complexed particle, which is central in this study, is then easily obtained through $n_L = L_T/d$. When the particles' FWHM becomes comparable to the instrument resolution, the domain size L and n_L determination becomes limited by resolution, and the real n_L is likely to be larger than the determined n_L. This occurs at $n_L \approx 60$.

3. Results and discussion

3.1. High membrane charge density

We studied the formation of un-PEGylated, and PEGylated (5 and 10% mol/mol) complexes in salt through two different pathways. In the first, the complexes are prepared in water, and salt is added 24 h later (referred to as the "after" method). In the second, the complexes are formed in saline conditions (referred to as the "before" method). We studied gradual additions of NaCl up to 150 mM (close to physiological concentration), and also DMEM, which is a culture media widely used in transfection efficiency (TE) studies, with salt concentration ≈150 mM. The influence of various compositional parameters from the complexes, such as membrane charge density (σ_M), positive to negative lipid/DNA charge ratio (ρ), and PEG2K molar fraction in the lipid membrane (%PEG2K) was also studied.

For all the conditions studied, liposomes and DNA associated with each other, as demonstrated with colocalization experiments. As can be seen in Fig. 1, in the absence of salt, discrete objects showing colocalized fluorescence of lipid and DNA dyes are seen for all the conditions at high σ_M and $\rho = 5$ (for the entire colocalization results, c.f. Fig. S1 in the supporting information (SI)). In the case of PEGylated complexes (middle and lower panels) the particles are only seen in the fluorescent mode (not in the DIC), which means they are smaller than ≈0.2 μm (the optical limit). When salt is added (before and after methods), the unPEGylated particles aggregate (due to Van de Waals attractions) into large objects, since the charge that was giving them colloidal stability is now screened. PEGylated particles, on the other hand, keep their small size. Nonetheless, no significant differences are observed between the two preparation methods at this (fluorescence microscopy) scale. The only exception is found for low σ_M at 10% PEG2K, where reduced colocalization is observed. The most important information obtained with this technique is that regardless of the preparation mode (before or after), lipid and DNA associate. Small-angle X-ray scattering (SAXS) was used to gain information into the nanostructure of these objects.

In Fig. 2 the radially averaged SAXS profiles from the high σ_M ($\approx 11 \times 10^{-3}$ e·Å^{-2}) complexes at $\rho = 3$ are shown for PEG2K = 0, 5 and 10%, and for various salt concentrations. In Fig. 3, SAXS profiles are shown for CL–DNA complexes at different charge ratios for fixed [NaCl] = 150 mM (comparable to the ionic strength of DMEM). The remaining SAXS data for high σ_M and low σ_M, different mol% PEG2K, and ρ, can be found on the supporting information (Figs. S2, S3 and S4).

As mentioned below (c.f. SAXS in methods section) most of the samples show a scattering pattern typical of lamellar complexes with DNA monolayers sandwiched between the lipid bilayers [7] (Fig. 2). On a larger length scale, the complexes consist of finite sized multilamellar particles with overall spherical shape (where the internal lamellar structure exhibits LC defects consisting either of stacks of bilayers with disclination defects, or spherulite-like onions with concentric layers) [7,8,51]. The average size of these particles is between 50 and 110 nm radius, as measured with dynamic light scattering [36].

When salt is added to complexes formed in water, or before complex formation, the L_α^C and DNA peak positions shift slightly, as expected from previous experiments [42] (c.f. Fig. S5 in SI). However, there is a higher shift to lower q in the complexes prepared in salt. Regardless of this, it is in the shape of the peaks that the highest differences between both methods of preparation are observed. As can be seen in Fig. 2, in the complexes where salt is added after complex formation, there are no strong changes in the scattering profiles as a function of salt concentration. Namely, the width of the main Bragg peak is not affected to any strong extent. This is true regardless of the amount of PEG2K. In contrast, for the complexes where salt is added before complex formation, one starts to see some slight broadening of the main Bragg peak at 100 mM NaCl for non-PEGylated complexes. For 5% PEG2K complexes, differences start to occur already at 50 mM NaCl, where the main Bragg peak seems now to be composed by two populations: one where the peak is narrow, and the other where the peak is broad. This trend continues as the salt concentration rises, and the broad population starts to be more predominant than the narrow one. At 150 mM NaCl the narrow population is barely visible, and when the media is DMEM,

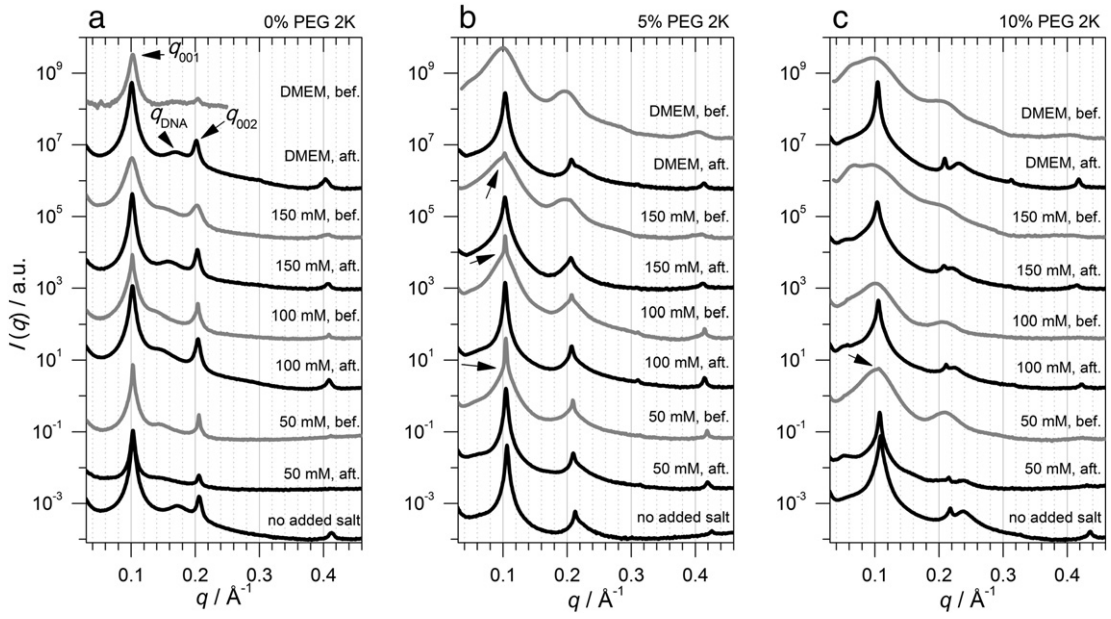

Fig. 2. SAXS profiles of high membrane charge density ($\sigma_M \approx 11 \times 10^{-3}$ e·Å^{-2}) complexes as a function of salt concentration and compared to DMEM, at $\rho = 3$, with (a) no PEG2K (DOTAP/DOPC; 80/20); (b) 5% PEG2K (DOTAP/DOPC/PEG2K; 80/15/5) and (c) 10% PEG2K (DOTAP/DOPC/PEG2K; 80/10/10). Black lines: complexes prepared in water ("after" method), with post added salt or DMEM; gray lines: complexes prepared in salt or DMEM ("before" method). Arrows in (a) indicate L_α^C peaks. Arrows in (b) and (c) indicate obvious overlap of narrow and broad L_α^C peaks. SAXS profiles obtained at the in-house instrument have a lower high-q range.

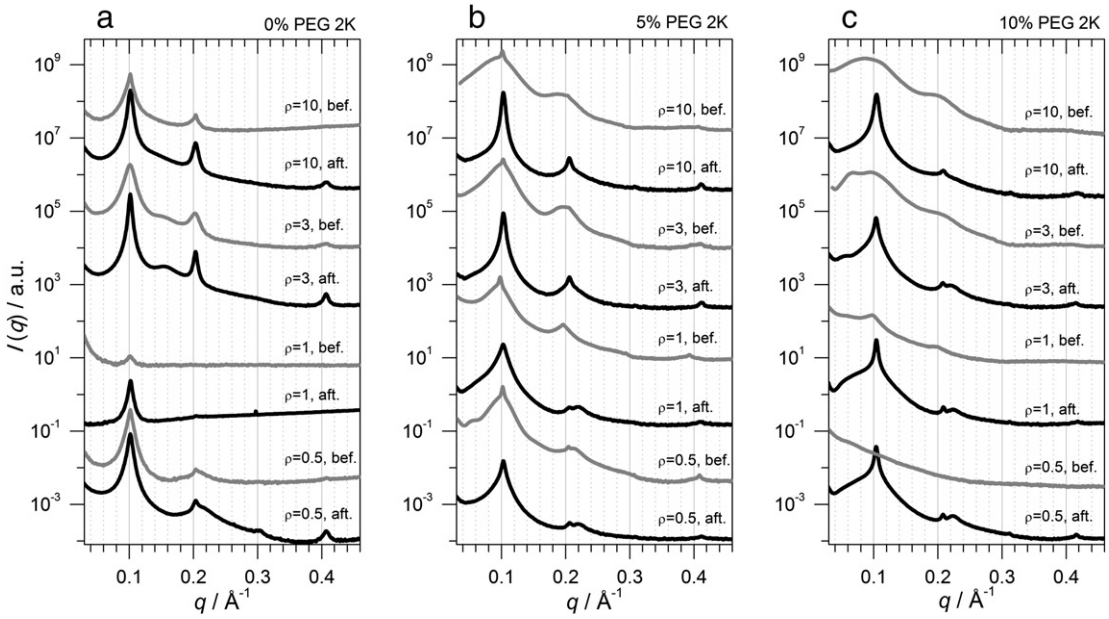

Fig. 3. SAXS profiles for positive ($\rho > 1$), isoelectric ($\rho = 1$) and negative ($\rho < 1$) complexes with high σ_M ($\sigma_M \approx 11 \times 10^{-3}$ e·Å^{-2}). (a) 0% PEG2K (DOTAP/DOPC; 80/20), (b) 5% PEG2K (DOTAP/DOPC/PEG2K; 80/15/5), and (c) 10% PEG2K (DOTAP/DOPC/PEG2K; 80/10/10). In all cases, NaCl concentration is 150 mM. Black lines: complexes prepared in water ("after" method); gray lines: complexes prepared in salt ("before" method).

only the broad peak is visible. When going to 10% PEG2K, the difference becomes even more dramatic for complexes where salt is added before complex formation. Now, at 50 mM NaCl, the main Bragg peak is essentially dominated by the broad population, with only a small fraction of the narrow one. At 100 mM NaCl the Bragg peak is extremely broad, with no signs of the narrow population. Also at this point (100 mM NaCl), a second broad peak at ca. $q \approx 0.06$ Å^{-1} starts to be visible. The intensity of this lower q peak keeps increasing as the salt concentration is increased, overlapping significantly with the original L_α^C broad peak at 150 mM NaCl and DMEM, making it more difficult to distinguish. This low q ($\approx$0.06 Å^{-1}) peak is also observed in solutions of liposomes in water and 150 mM salt (in salt the peak becomes narrower), without DNA (c.f. Fig. S6 in SI). Therefore, this peak does not correspond to lipid-DNA L_α^C particles. The fact that the signal from lipid alone becomes comparable to the L_α^C peak indicates that for these conditions, complexation is not as complete as in the remaining ones (lower %PEG2K or lower salt).

These global trends are also observed for $\rho = 0.5$, 1 and 10 complexes (Fig. 3). The complexes where salt is added after complex formation have, in general, narrower Bragg peaks than the complexes where salt is added before. Each of these narrow or broad peaks is stable with time, for at least two months. The exception occurs at 10% PEG2K $\rho = 0.5$, where complexation does not seem to occur. It is also visible that in PEGylated complexes, on the negative and neutral side ($\rho = 0.5$ and 1) particles have slightly broader peaks than $\rho = 3$ and 10, when salt is added after. The $\approx$0.06 Å^{-1} peak is also seen to be more clear at high ρ, which is expected since lipid is present in higher amounts.

At low σ_M (Figs. S3 and S4 in SI) the same general trends are observed for un-PEGylated complexes and PEGylated complexes at low salt (up to 100 mM). At that point, as we move to 150 mM NaCl, a new regime seems to be entered, with the scattering pattern attributed to L_α^C being replaced with novel features. This new regime will be discussed further below.

3.2. Fits of SAXS data to theoretical model

The differences in the shape of the Bragg peaks can be better quantified with the means of line-shape analysis. Here we use Eq. (1) to fit the main lamellar peak, which yields an accurate estimate of the peak position (q_{001}), lamellar spacing (d) and number of layers (n_L) in the complex.

Fig. 4 shows some representative fittings on narrow and two-population peaks. Fig. 4a is a typical example of a narrow peak (hence with large n_L). The fitting is very good in most of the data range, but fails slightly near the tail region. There are two main reasons for this. In the first place, Eq. (1) was deduced for the case of stacked fluid layers (lamellar phase). Since in the L_α^C phase there is also DNA sandwiched between bilayers in the aqueous region, this causes some modifications in the Hamiltonian of the bilayer sheets. Therefore it is not surprising that some deviations occur, especially at large $|q-q_{001}|$, where the modulations of the bilayer shape due to coupling to the DNA monolayer may be more important, and which is indeed observed. At low $|q-q_{001}|$, which is the most important region in terms of obtaining the number of layers n_L, the fitting is very good. In the second place, in the fitting procedure a single n_L (or L) is being assumed, which is an approximation. Indeed, there should be some polydispersity in n_L, which would also contribute to a slightly different shape. In order to include polydispersity effects, either a thorough characterization of the complexes with cryo-TEM would need to be performed, which is out of the scope of this work, or a distribution function with standard deviation would need to be included in Eq. (1), introducing one more fitting parameter. Since the fitting with a single n_L is very good in most of the data range, and always reproduces well the peak's full-width-at-half-maximum (FWHM), we prefer to avoid that extra complication. In some samples, there is an obvious coexistence of two peaks (c.f. arrows in Fig. 2b and c). In these cases, and since the coexistence is obvious by visual inspection, the data is fitted as a sum of two peaks (c.f. Fig. 4b).

In Fig. 5, the fitting results are shown for the three PEG2K compositions (0, 5 and 10%), for high and low σ_M at $\rho = 3$, as a function of salt (c.f. Fig. S7 in SI for the fitting results at $\rho = 0.5$). The overall picture obtained by examining the scattering patterns in Figs. 2 and 3 is confirmed. As can be seen, complexes initially prepared in water have about 20–40 layers (independent of the PEG2K coverage) and do not present significant changes in the number of lamellar layers as the salt concentration is increased. In contrast, when the complexes are prepared in saline conditions, the differences are striking. For non-PEGylated complexes, this difference is not yet very significant.

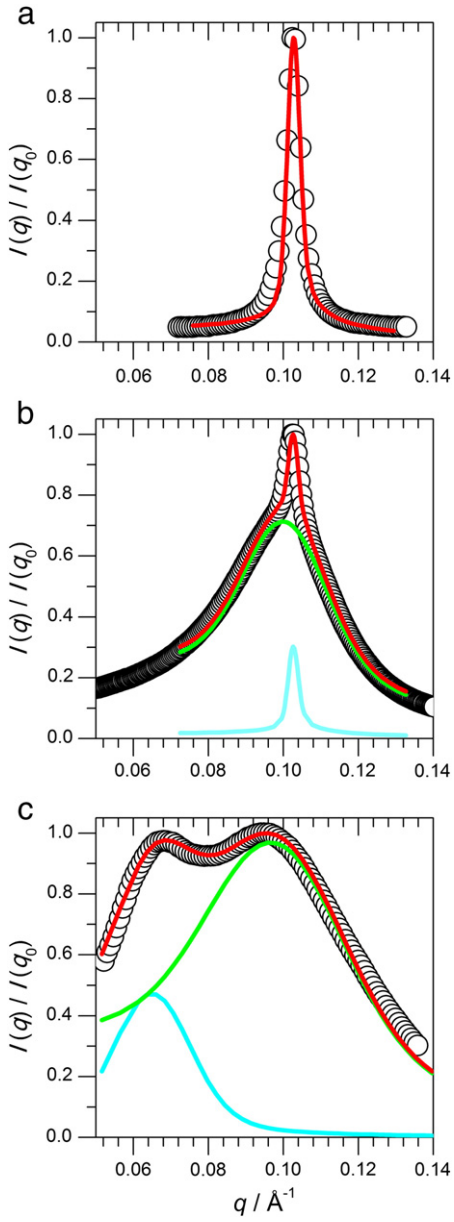

Fig. 4. Representative figs. of the SAXS data fitting with the Caillè equation for high σ_M ($\approx 11 \times 10^{-3}$ e·Å^{-2}) complexes. (a) 0% PEG2K (DOTAP/DOPC; 80/20), $\rho = 3$, 50 mM NaCl added after. (b) 5% PEG2K (DOTAP/DOPC/PEG2K; 80/15/5), $\rho = 3$, 150 mM NaCl added before. (c) 10% PEG2K (DOTAP/DOPC/PEG2K; 80/10/10), $\rho = 3$, 150 mM NaCl added before. In the cases where two peaks are present, the green and cyano lines represent the individual peak fittings, and the red line their sum. (b) is a typical example where the coexistence of two L_α^C populations (or two overlapped peaks) is obvious. (c) is a typical example where a peak at low q ($\approx$0.06 Å^{-1}) overlapping with the L_α^C peak is observed.

The number of layers in the non-PEGylated complexes prepared in salt is slightly larger for 50 and 100 mM NaCl, and smaller for 150 mM NaCl and DMEM. This nearly pathway-independent complex formation result indicates that such complexes are at, or near equilibrium. In PEGylated complexes the differences between both methods of preparation are much larger, indicative of the presence of kinetically trapped complexes. In 5% PEG2K complexes, two populations of particles are found when the complexes are formed under saline conditions. One population with a large number of layers ($n_L \approx$ 40–50), gives rise to the narrow peak, and another population with a low number of layers ($n_L \approx 4$), gives rise to the broad peak. The relative areas of each peak (obtained in the fitting) roughly indicate the relative volume of high and low n_L particles, shown as the line in Fig. 5 and S7. As can be seen, even though both particle sizes are constant (i.e. the number of layers), the population with low n_L is increasing at the expense of the population with large n_L as the salt concentration rises.

As the amount of PEG2K is increased to 10%, the differences between both methods increase even further. Now at 50 mM NaCl, the large n_L population is barely seen, and furthermore, has only about 14 layers, as compared to 5% PEG2K. At 100 mM NaCl, all the complexes are already very loose with n_L equal to 3 or lower. The peak at low $q \approx 0.06$ Å^{-1}, discussed before, also becomes visible at this point, overlapping with the L_α^C peak. For this reason, we fit both peaks simultaneously (sum of both peaks), in order to deconvolute them (Fig. 4c).

In some complexes prepared in salt (mainly at 5% PEG2K), the observation of the coexistence of two populations (high n_L coexisting with low n_L) instead of one population with average n_L is not trivial. One hypothesis that can justify this behavior would be the existence of some polydispersity in the amount of PEG2K in the membranes. Hence, bilayers richer in PEG2K would behave more as the 10% PEG2K case, in which a smaller n_L is observed, whereas bilayers poorer in PEG2K would behave more as 0% PEG2K, in which a larger n_L is also observed. Alternatively, the low population complex state may be kinetically trapped.

These overall trends are similar for $\rho = 0.5$ (c.f. supporting information), and seem to indicate that it is the combination of PEG2K plus salinity of the medium that affects complex formation, since as was seen, in the absence of salt, high membrane charge density complexes form with 5 and 10% PEG2K, and non-PEGylated complexes also form at 150 mM NaCl and DMEM. As will be further discussed below, these observations seem to indicate that at low salt the electrostatic attraction between cationic liposome and DNA is still dominant over the repulsive steric force of PEG2K. However, since the most common effect of salt is to screen electrostatic interactions, weakening them, at high salt concentrations the magnitude of the electrostatic force becomes comparable to the steric repulsion, leading to a progressive destabilization of PEGylated complexes. The fact that complexes formed in water and transferred to saline media hold their structure seems to indicate that complexes are equilibrium structures. So, the destabilizing effect of combined PEG2K and salt is probably due to the kinetic barrier for complex formation, but not very important in the final equilibrium energy of the complexes.

3.3. Low membrane charge density and a new regime

Overall, at low σ_M, complexes follow a similar trend to the high σ_M ones, i.e. complexes where salt is added after have a large number of lamellar layers when compared to the ones prepared already in salt (Figs. S3, S4 and S7 in SI). In this case, however, since the electrostatics (which favor complex formation) are further weakened (lower σ_M), addition of salt has an even stronger effect. This also brings some additional effects, not visible at high σ_M. Most notably, a new regime where complex formation does not occur is entered for 10% PEG2K, when DNA and cationic liposome are mixed in the presence of high salt.

Non-PEGylated complexes (c.f. $\rho = 3$ in Fig. 5d and $\rho = 0.5$ in Fig. S7d in SI) have a large number of layers when salt is added after ($n_L \approx$ 30–60). This number is significantly higher than for the high σ_M homologues. This does not mean, however, that non-PEGylated low σ_M complexes are more stable than the high σ_M ones. The higher n_L likely results from a weaker colloidal stability of the low σ_M particles, which results in some aggregation and fusion between complexes, leading to a higher n_L. In the cases where salt is added before complex formation, n_L starts to drop already at 100 mM NaCl, whereas in high σ_M complexes this only occurs at 150 mM. Also, n_L at this point is significantly lower than at high σ_M. This is true for $\rho = 3$ and $\rho = 0.5$.

PEGylated complexes have a different behavior at low σ_M. When complexes are prepared in water and salt is added afterwards, the complexes are stable for 5% PEG2K, but for 10% PEG2K, the intensity of the

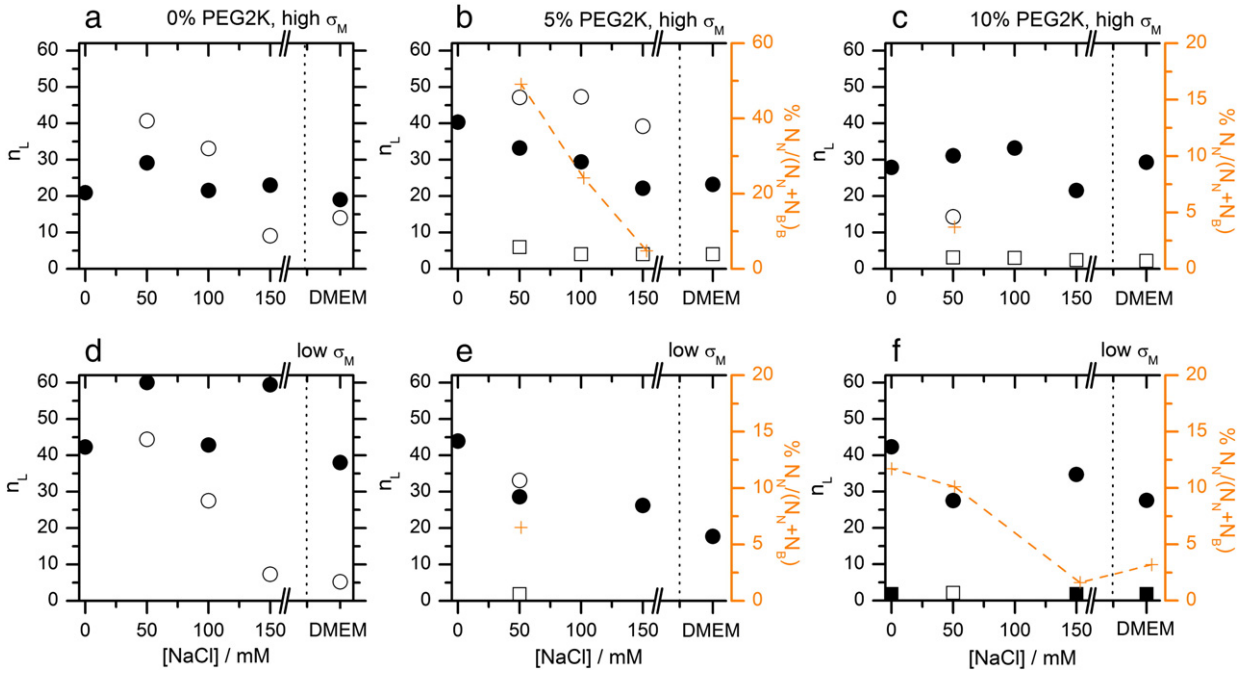

Fig. 5. SAXS-fitting results showing the average number of layers (n_L) in high ($\sigma_M \approx 11 \times 10^{-3}$ e·Å^{-2}) and low σ_M ($\approx 4 \times 10^{-3}$ e·Å^{-2}) PEG2K–CL–DNA positive complexes ($\rho = 3$) prepared with salt (or DMEM) added either after (filled symbols) or before (open symbols) complex formation. Some samples showed coexistence of two populations (c.f. Fig. 2) with different average number of layers. In these cases, circles and squares represent the narrow and broad populations respectively, and the orange cross and line represents the relative fraction of the narrow peak area over the sum of both narrow and broad peak areas ($\%N_N/(N_N + N_B)$). (a) 0% PEG2K (DOTAP/DOPC; 80/20), high σ_M, $\rho = 3$; (b) 5% PEG2K (DOTAP/DOPC/PEG2K; 80/15/5), high σ_M, $\rho = 3$; (c) 10% PEG2K (DOTAP/DOPC/PEG2K; 80/10/10), high σ_M, $\rho = 3$; (d) 0% PEG2K (DOTAP/DOPC; 30/70), low σ_M, $\rho = 3$; (e) 5% PEG2K (DOTAP/DOPC/PEG2K; 30/65/5), low σ_M, $\rho = 3$; (f) 10% PEG2K (DOTAP/DOPC/PEG2K; 30/60/10), low σ_M, $\rho = 3$. In (d), the two particles with $n_L \approx 60$ are resolution limited, and their real n_L can be larger.

main Bragg peak compared to the baseline is notably smaller. As can be seen, especially at $\rho = 0.5$ (Fig. 6), 10% PEG2K complexes seem to be divided into two populations when prepared in water ("after" method), as the Bragg peak for the L_α^C phase seems a superposition of one narrow and one broad peak. This is similar to the behavior observed at high σ_M with 5% PEG2K complexes when prepared in salt. In addition, there is also a peak at lower q ($\approx$0.07 Å^{-1}),[1] that we attribute to excess lipid, which also suggests that under these conditions of high PEG2K mol% and low σ_M, complexation is not as complete as in the remaining compositions. It is however, when complexes are prepared in salt that the major differences are observed.

When prepared in salt ("before" method), the behavior of 5% and 10% PEG2K systems becomes significantly different, with ρ starting to play a more important role. At 50 mM salt, 5% PEG2K ($\rho = 3$ and $\rho = 0.5$) systems show a narrow L_α^C peak coexisting with a broad L_α^C peak, and another broad peak at q close to 0.07 Å^{-1} (Figs. S4 and S5, SI). At 100 mM salt and above, $\rho = 3$ and $\rho = 0.5$ complexes start to behave differently. For $\rho = 3$ the L_α^C peak one would expect to observe at $q \approx 0.09$ Å^{-1} (from comparison with the "after" method) is replaced by two convoluted broad peaks at $q \approx 0.07$ and $q \approx 0.11$ Å^{-1}, and another broad peak (probably the harmonic of the first two peaks, convoluted into one peak) at $q \approx 0.17$ Å^{-1}. At $\rho = 0.5$ the L_α^C broad peak ($q \approx 0.09$ Å^{-1}) remains throughout the whole salt range. These results are confirmed if one looks also at the dependency of ρ for fixed 150 mM salt and DMEM (Fig. 7). As can be seen, in both salt and DMEM cases, the L_α^C broad peak is observed at $\rho = 0.5$. At $\rho = 1$ the L_α^C peak is still present, but now, it seems overlapping with another peak at lower q. At $\rho = 3$ the L_α^C peak is replaced by the two convoluted peaks mentioned before. In Fig. 7c the signal from the pellets is compared with the supernatant (which is likely to be composed of excess lipid alone). As can be seen, the two overlapped broad peaks are also observed in the supernatant, for all ρ. This suggests that the two broad peaks are coming from the lipid alone, and not from complexes. In addition, as can be seen in Fig. S6, liposomes of low σ_M with 5% PEG2K (no DNA), which are stable in water, and show no clouding in 150 mM NaCl, develop two broad peaks when transferred to salt. It is not entirely clear if this change in scattering caused by salt is due to a change in the form factor or structure factor (or even both), but importantly, these two peaks are similar to what is observed in the CL–DNA systems. Hence, these two main peaks observed are from the lipid alone. The q peak positions of the two peaks with or without DNA are not exactly the same, which is probably a result of the different solution properties (e.g. differences in the solvent osmotic pressure, caused by DNA).

Since the L_α^C peak is observed at $\rho = 0.5$, it seems plausible that it is still present at $\rho = 3$, but due to the much higher amount of lipid (higher ρ), its signal is not visible. Colocalization also suggests this hypothesis (Fig. S1 in SI). Even though colocalization cannot clearly differentiate between real complexes or the case of just association/aggregation between lipid and DNA, the fact that the colocalized intensity in this system is similar to most of the other systems with exception of 10% PEG2K system at low σ_M (which will be discussed below), suggests that indeed complexes also form at $\rho = 3$ and $\rho = 5$.

At 10% PEG2K a similar behavior is observed, but again, like in the high σ_M case, the higher amount of polymer induces more drastic changes in the behavior. At low salt (50 mM for $\rho = 3$; 50 and 100 mM for $\rho = 0.5$), coexistence of the L_α^C peak ($q \approx 0.087$ Å^{-1}, identical to the complexes where salt is added after) with two more broad peaks is still observed (Figs. 6, S3 and S4). However, at 150 mM NaCl and DMEM the L_α^C peak is not visible anymore, and the broad peaks are replaced by three sharp peaks with $q_{00l}/q_{001} = 1,2,3$, in agreement with a lamellar phase. Also here this sharp lamellar phase is more clear for $\rho = 3$, than $\rho = 0.5$, since in the former, the sharp lamellar

[1] For the estimation of n_L we fit the 3 peaks simultaneously so that their individual contributions can be decoupled. The existence of the broad peak is not as obvious as in the preceding cases due to the presence of the peak at $q \approx 0.07$ Å^{-1}. Nonetheless, we decided to include the n_L values obtained in the fitting of the L_α^C broad peak ($q \approx 0.09$ Å^{-1}) in Figs. 5 and S7, even if here this value is more uncertain.

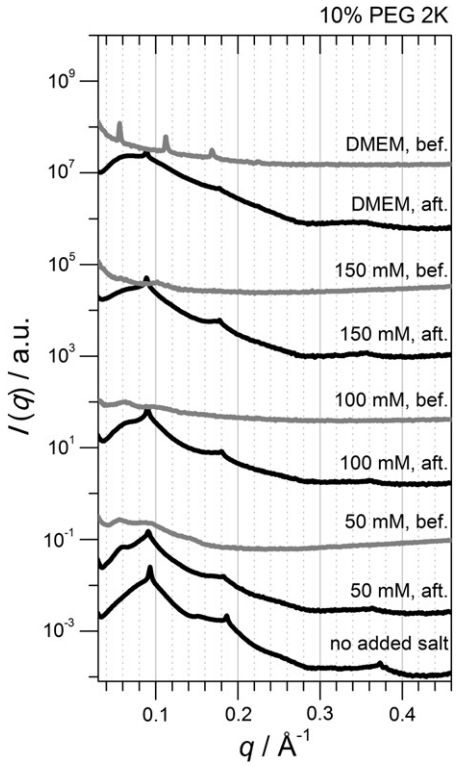

Fig. 6. SAXS profiles of low σ_M ($\approx 4 \times 10^{-3}$ e·Å^{-2}), 10% PEG2K (DOTAP/DOPC/PEG2K; 30/60/10) systems as a function of salt concentration and compared to DMEM, at $\rho = 0.5$. Black lines: complexes prepared in water ("after" method), with salt or DMEM added post complexation; gray lines: complexes prepared in salt or DMEM ("before" method). The L_α^C peak is clearly visible in the complexes where salt is added after complexation. In this case, however, it is divided in one narrow peak, overlaid on a broad peak, indicating coexistence of particles with large and small n_L. In the complexes where 50 mM salt is added before, there is still a reminiscent broad peak from the L_α^C phase surrounded by two more broad peaks at low and high q. At higher salt concentrations, the L_α^C phase is not visible any longer (at least at $q \approx 0.09$ Å^{-1}, as in the "after" complexes). At 100 mM NaCl, there is one broad peak at $q \approx 0.1$ Å^{-1}, which could result from complexation of DNA with demixed lipid rich in DOTAP. In DMEM, a lamellar phase of essentially non-complexed lipid with spacing controlled by the amount of PEG2K is observed.

phase is entered at 150 mM salt, whereas for the later the sharp lamellar phase only appears in DMEM. Also in this case, the extra peak that starts appearing at low q and low salt is visible also in the pure lipid–salt system (Fig. S6), indicating that rather than complexing with DNA, the lipid is undergoing a different pathway. The scenario of aggregation into multilamellar vesicles seems a strong hypothesis. The high PEG2K surface coverage should be enough to prevent aggregation of these liposomes, so one hypothesis could be the aggregation being facilitated by a minute amount of DNA, that would help bring the liposomes together, but not induce a strong enough interaction to originate a complex with the typical water layer thickness of 25 Å. Instead, the spacing of these multilamellar vesicles would be controlled by the amount of PEG2K in the membranes. The peak position at $q \approx 0.06$ Å^{-1} corresponds to a real space dimension of ≈10 nm, which correlates well with the sum of the bilayer thickness (≈4 nm) plus two times PEG2K R_g (2×3.5 nm). The sharp peaks reflect a large number of layers: $n_L \approx 10$–20. In the colocalization experiments, a reduced (but not negligible) colocalization was observed for 10% PEG2K when compared with the remaining systems (c.f. Figs. 1 and S1 in SI). This indicates that under these extreme conditions, DNA and lipid still partially associate or aggregate, but complexation involving the rearrangement and formation of the L_α^C phase has not occurred.

In the 10% PEG2K $\rho = 0.5$ system, it is unclear if the second peak at $q \approx 0.1$ Å^{-1} found for 100 mM NaCl could correspond to a L_α^C or not. The spacing $d \approx 6.2$ nm is similar to the one found for high σ_M complexes (5.7–6.3 nm), which could correspond to a scenario where some lipid demixing into domains richer in DOTAP (or poorer in PEG2K) had occurred, driving some complexation with a different membrane composition to the one expected. For this reason, we tentatively attribute this phase to the L_α^C noting that some lipid demixing may have occurred.

3.4. Summary of the experimental results

These experimental observations can be compiled in a phase diagram scheme (which includes kinetically trapped states) reflecting the overall phase behavior at high salt (Fig. 8). As is patent, the phase behavior is modulated by (i) the preparation method; (ii) amount of PEG2K; (iii) membrane charge density (σ_M); and (iv) amount of salt. Complexes formed in water, with salt added afterwards always form stable complexes (the only partial exception is at low σ_M with 10% PEG2K, where two n_L populations are obtained, instead of just one). When complexes are formed in the presence of salt, their structure is highly affected. At high σ_M, complexes still form, but they are affected by the amount of PEG2K and salt. At low σ_M, complexation with PEGylated liposomes becomes weaker for increasing amounts of salt. This is reflected in the signal from the liposomes alone, which do not complex. At 150 mM and DMEM, 5% PEG2K systems only show complexes at $\rho = 0.5$ and $\rho = 1$. At $\rho = 3$ the lipid signal completely obscures any hypothetical signal from complexes, even though their presence is suggested also by colocalization. At high salt conditions, the 10% PEG2K system does not show scattering signal attributable to complexes. A lamellar phase (likely in the form of multilamellar vesicles) nearly depleted of DNA is observed instead.

The fact that both types of complexes are stable through time suggests that this L_α^C phase is the equilibrium structure. The final size distribution (namely the number of layers n_L) is however controlled kinetically.

4. Modeling and discussion

Although the main driving force for complexation is thought to be simply the high entropic gain due to the release of the inorganic counterions when DNA and cationic lipid neutralize each other [7,40,41], the actual mechanism leading to the final compacted state is presumably more complex, and involves several steps. It has been suggested [51–54] that when the cationic liposomes and DNA are first mixed, the first step involves coating of the liposomes with DNA. We hypothesize that the degree of coating will be highly polydisperse (which will reflect on a χ parameter, to be defined later), giving rise to a broad distribution of liposome charges, from positive to negatively overcharged. In a subsequent step, a second liposome (coated or naked in DNA) attaches to the first, forming a lipid-DNA-lipid contact area. Here, we also hypothesize that attachment will be favored between liposomes overcharged with DNA (hence negative) with liposomes barely coated, since these conditions should maximize electrostatic attraction and counterion release. After these two initial steps, the two liposomes can either fuse, or the second can break and roll over the first, forming a liposome with two bilayers. This second process can continue n more steps, giving rise to a CL–DNA complex with approximately n layers.

By adding PEG2K to the lipid bilayers, we believe that the most profound effects will be on (i) opposing the attachment of the second (partially coated or uncoated) liposome to the first (coated) liposome, and on (ii) the coating of the second ruptured liposome over the first (intact) liposome. Both of these steps involve confinement of PEG2K to a smaller region, leading to a steric repulsive force opposing them, and should constitute rate-limiting steps in PEG2K–CL–DNA complexation. Hence, the formation of PEG2K–CL–DNA complexes results mainly from a balance of electrostatic (here, mainly of attractive nature); and steric forces (repulsive). While the second process, involving vesicle rupture and curvature change, seems somewhat complicated to model using simple mean-field approaches, the first process, attachment, can be modeled (assuming some approximations) by

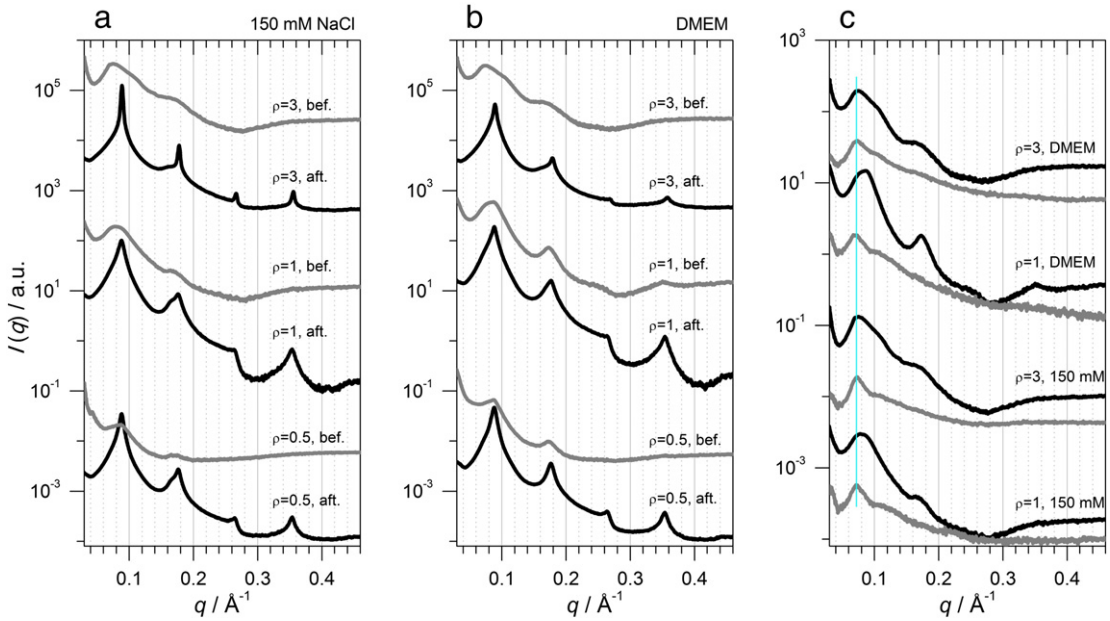

Fig. 7. SAXS profiles for positive ($\rho > 1$), isoelectric ($\rho = 1$) and negative ($\rho < 1$) complexes of low σ_M ($\approx 4 \times 10^{-3}$ e·Å^{-2}) and 5% PEG2K (DOTAP/DOPC/PEG2K; 30/65/5) in (a) 150 mM NaCl; and (b) DMEM. Black lines: complexes prepared in water ("after" method); gray lines: complexes prepared in salt ("before" method). In (c) the $\rho = 1$ and $\rho = 3$ complexes from the "before" method are plotted together with the supernatant (gray lines). The blue line is a guide for the eye, centered at the q of the low q (≈ 0.7 Å^{-1}) peak. As can be confirmed, this peak is also present in the supernatant, and is more evident at $\rho = 3$ where the L_α^C peak at $q \approx 0.9$ Å^{-1} has already vanished. At $\rho = 1$ there are already some traces of the low q peak.

calculating the electrostatic attraction between two oppositely charged surfaces (within a Poisson Boltzmann framework) and steric repulsion caused by polymer confinement.

To model this process, we consider two infinite flat surfaces, representing the cationic lipid monolayers (i.e. half of the lipid bilayers — Fig. 9), separated by a water layer of thickness d_w, and Debye screening length λ_D (c.f. the supporting information for details on how these quantities are calculated and additional comments). The lipid monolayers can be partially or fully covered with DNA rods (or base pairs). Each DNA base pair bears two negative charges, which neutralize two charges in the lipid monolayer. In this model, as a simplification, the total amount of negative and positive charges is the same, corresponding to a situation of isoelectric (or neutral) complexes ($\rho = 1$). This also implies that the total charge in one side of the cell (lipid monolayer plus any additional absorbed DNA rod) is equal in magnitude to the total charge in the other side of the cell, but with opposite signs.[2]

The electrostatic energy is calculated using a Poisson–Boltzmann (PB) model, developed by Meier–Koll, Fleck and Von Grünberg [55], accounting for the Coulomb interaction between oppositely charged species, and importantly, accounting for the positive entropy gain due to counterion release (cf. supporting information for the details).

The attraction between two oppositely charged surfaces is maximum when one liposome is free of DNA, and the other is fully coated with DNA, i.e. each positive charge has a DNA base pair attached to it, which fully inverts the charge of the monolayer to negative (the liposome is 100% overcharged in the outer monolayer). Even though this situation would be barely seen (it is unlikely that DNA will fully absorb on one cationic liposome, due to electrostatic repulsion between the neighboring rods), it would correspond well to the case of a liposome with excess DNA, attaching to a DNA-free liposome. If, as can be seen in Fig. 9, one DNA rod is shifted to the positive surface, the effective charge density ($\Delta\sigma_M = \chi\sigma_M$) of each monolayer will decrease by a factor of χ, defined as the cationic monolayer-DNA neutralization factor ($\chi = (n_{CL}-2n_{DNA})/n_{CL}$, where n_{CL} stands for the number of positive charges in the monolayer and n_{DNA} stands for the number of transferred DNA base pairs), and therefore, the attractive force will be reduced. This would correspond to a situation where one liposome with negative charge (partially overcharged with DNA) would attach to a liposome with net positive charge (partially coated with DNA, but still with excess positive charge). As soon as DNA and cationic liposomes are mixed in solution, a distribution with all of these states should occur, i.e. some liposomes with excess DNA (negatively charged, $\chi > 0.5$), some neutral ($\chi = 0.5$), and some with deficit of DNA (positively charged, $\chi < 0.5$). Therefore we calculate the electrostatic interaction for different values of χ, in an attempt to capture this polydispersity in liposome charge. Another factor that should increase the variability of χ is the polydispersity of calf thymus DNA. The χ parameter is therefore crucial in the used model. The effective membrane charge density $\Delta\sigma_M$ is calculated by $\Delta\sigma_M = e\cdot\chi/(d_{DNA}\cdot l_{bp})$, with e the electron's charge. d_{DNA} is fixed to 27.3 Å (the measured value at high σ_M and $\rho = 1$). Since χ is varied systematically, the low σ_M complexes are covered (effectively, low σ_M with $\chi = 1$ is identical to high σ_M with $\chi = 0.6$).

When considering the steric repulsion, two regimes can be considered depending on the amount of PEG2K on the liposome surface: (i) the mushroom regime, when the distance between nearest neighbor PEG2K chains is larger than the radius of gyration (R_g) of each chain (and therefore, the PEG2K chains do not overlap); and (ii) the brush regime, when this distance is smaller than the polymer R_g, leading to a nearly full coverage of the liposome surface, and to an expansion of the polymer outwards of the liposome to minimize the overlapping of the chains [31]. Through geometric arguments (c.f.

[2] *Two* oppositely charged surfaces are always attractive if the magnitude of their membrane charge densities is equal. If the magnitude of the membrane charge density is different, the surfaces will have a long range attraction, but due to the charge density mismatch, the surfaces cannot fully neutralize each other, and a remaining amount of counterions will remain in the space between both surfaces, giving rise to a short-range osmotic repulsion. As a simplification in our model, we only consider oppositely charged surfaces with the same charge density ($\sigma^+ = -\sigma^-$). We believe this is a reasonable approximation due to the fact that even though at the beginning, most approaching surfaces will have different charge densities, the absorbed DNA (which is packed in a 2-D smectic liquid crystal) can rearrange in the lipid bilayer, allowing for a "good" matching between both membrane charge densities. This would correspond to a case where both membranes have equal charge densities but opposite sign, yielding a purely attractive PB interaction.

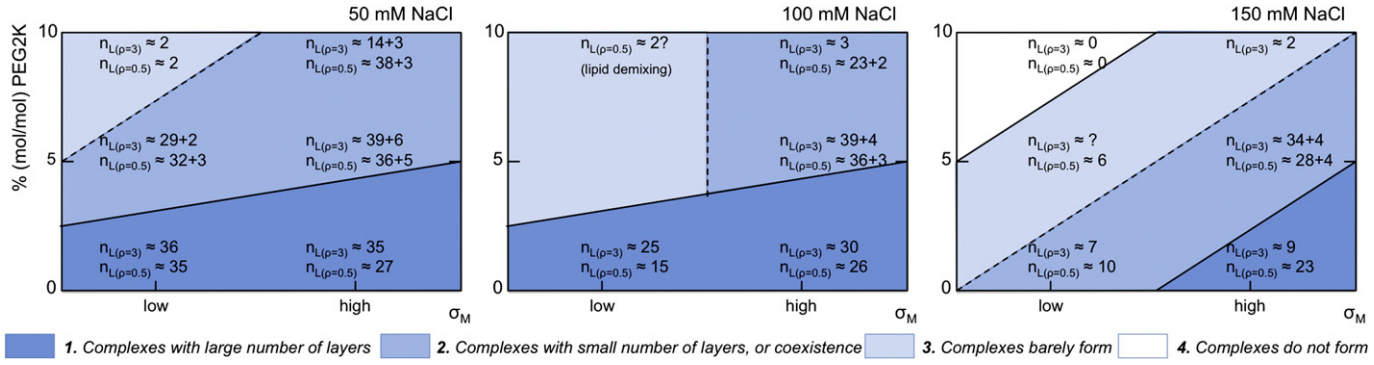

Fig. 8. Schematic of the phase behavior (including kinetically trapped states of complexes) at 50, 100 and 150 mM NaCl for positive ($\rho = 3$) and negative ($\rho = 0.5$) complexes. Complexes where salt is added after complexation always form in this salt range, so the different areas of the diagram correspond only to the complexes prepared in the presence of salt ("before" method). In region 1, complexes form with a large number of layers. In region two, complexes form with a smaller number of layers (but still significant). Very often, coexistence of two populations is observed, with the population with small number of layers dominating. Region 3 — "complexes barely form" is used for the regions where n_L is ≈2, and when there are differences between $\rho = 0.5$ and $\rho = 3$. In region 4, complex formation is not observed, even though it is not clear if a minute amount of complexes may form, but stay undetected by SAXS. Some colocalization is observed in this region, which could indicate some aggregation between both lipid and liposomes, although, without the structural rearrangements associated with complex formation. In some cases, the region assignment is tentative (e.g. 5% and 10% PEG2K at low σ_M and 100 mM NaCl). As can be seen in the figures, the non-equilibrium phase behavior is controlled mainly by the amount of salt, %PEG2K and σ_M, in a way that could be expected by considering that the main contribution to complex formation is electrostatics (which are screened by salt), and the main force opposing complexation is the steric repulsion provided by PEG2K. Data for 5% PEG2K at 100 mM salt is missing, but by comparison with 50 and 150 mM areas, we attribute this region to "complexes barely form". For 10% PEG2K at 100 mM, the main (broad peak) occurs at 0.1 $Å^{-1}$ which is higher than what would be expected for these complexes (should be ≈0.09 $Å^{-1}$). This could either indicate complexation of DNA with lipid richer in DOTAP (by resemblance with the high σ_M case, which could occur if there is partial demixing of lipid), or a different phase.

supporting information), the distance s between PEG2K chains is estimated to be 40 Å for the 5% PEG2K complexes, and 28 Å for the 10% ones. Since R_g is 35 Å for PEG2K, the 5% PEG2K complexes are in the mushroom regime, and the 10% ones are in the brush regime.

The steric repulsive potential from PEG2K in the mushroom regime can be estimated for a theta solvent by [31]

$$V_{\text{mushroom}} = \frac{36}{s^2} k_B T \exp\left(-\frac{d_w}{R_g}\right). \quad (3)$$

Since water is a good solvent, the potential as given by Eq. (3) is somewhat underestimated. The steric repulsive energy arising from PEG2K in the brush regime can be estimated for a good solvent by [31,56]:

$$V_{\text{brush}} = \frac{k_B T}{s^3}\left\{\left(\frac{8L_{PEG}}{5}\right)\left(\frac{2L_{PEG}}{d_w}\right)^{(5/4)} - \left(\frac{4d_w}{7}\right)\left(\frac{d_w}{2L_{PEG}}\right)^{(3/4)}\right\} \quad (4)$$

where L_{PEG} is the length of the polymer brush extending outward from the liposome surface. Here, L_{PEG} is estimated to be 65 Å (c.f. supporting information for details).

Van de Waals attractive and hydration repulsive forces were considered, but not included in this model, since they are not very relevant at membrane separations larger than ≈25 Å. Furthermore, the salt and polymer effects addressed in this problem should have little importance

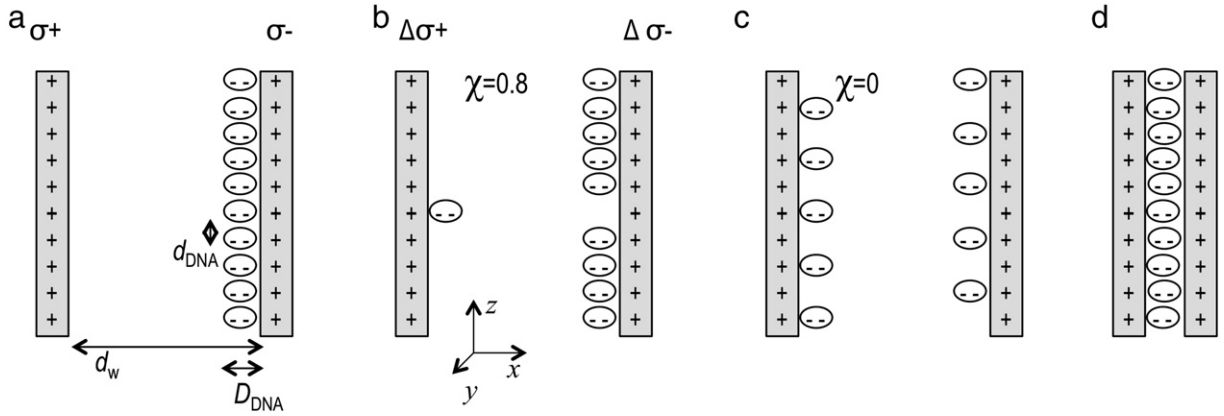

Fig. 9. Simplified model for two liposomes approaching each other. Each gray rectangle with positive charges represents a cationic lipid outer monolayer, and each white ellipse represents a DNA rod. In this simplified model, the membranes only attract each other if there is a net charge between them. For this reason, in (a), the monolayer on the right is entirely covered by DNA rods, having a negative charge density (σ^-), while the one on the left is depleted of DNA, having a positive charge density (σ^+). The net charge inside the cell is zero, and each monolayer has exactly the same charge of the other, but with opposite sign ($\sigma^- = -\sigma^+$). In (b) one DNA rod is transferred from one monolayer to the other. The net charge inside the cell is still zero, and each monolayer still has the same charge of the other with opposite sign. The main difference is that now, the net charge of each monolayer is decreased by a factor of χ, ($\chi = (n\text{CL}-2n_{\text{DNA}})/n\text{CL}$, where nCL stands for the number of positive charges in the monolayer and n_{DNA} stands for the number of transferred DNA base pairs), to a value of $\Delta\sigma$ ($\Delta\sigma = \chi\sigma$), resulting in a weaker attraction. (a) would mimic well the extreme situation where a liposome saturated with DNA approaches a "naked" liposome, while (b) would mimic a situation where two partially DNA-coated liposomes approach each other. One negatively charged (with excess DNA), and the other positively charged. In (c), each monolayer is neutralized by DNA base pairs, resulting in a net zero charge density and no long-range attraction in the PB model. In (d) the final state of each of the (a–c) surfaces at $d_w = 25$ Å is shown, which corresponds to the L_α^C phase.

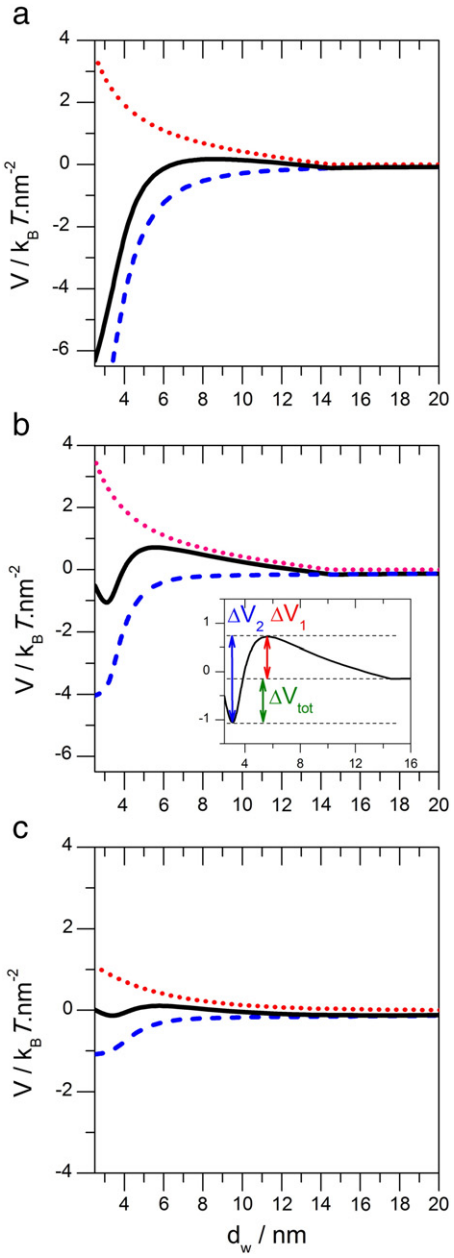

Fig. 10. Electrostatic attraction (dashed blue line), steric repulsion (doted red line) and overall interaction (black line) potentials between two oppositely charged membranes as a function of membrane separation for different values of cationic monolayer-DNA neutralization values (χ) and C_s. (a) $\chi = 0.9$, no added salt, brush regime (10% PEG2K); (b) $\chi = 0.9$, 100 mM salt, brush regime (10% PEG2K); and (c) $\chi = 0.4$, 100 mM salt, mushroom regime (5% PEG2K). The inset in (b) shows a magnification of the overall potential, showing the energetic barriers ΔV_1 and ΔV_2, as well as the energy difference between the two minima (ΔV_{tot}).

for these two forces, for which it is better to ignore them, than to include them in the model and have to include more fitting parameters.

Fig. 10 shows the resulting potentials of interaction for particles with $\chi = 0.9$ with no added salt (only counterions) and 100 mM NaCl for the brush regime (10% PEG2K), and $\chi = 0.4$ and 100 mM NaCl for the mushroom regime (5% PEG2K). The influence of electrostatic and steric interactions becomes immediately evident. The steric potential starts at zero, and when d_w becomes smaller than twice the brush length ($L_{PEG} = 6.5$ nm), it starts to rise, reaching a value of about 3.5 $kT \cdot nm^{-2}$ at $d_w = 25$ Å (Fig. 10a). The mushroom potential is much weaker as can be seen in Fig. 10c. The electrostatic interaction is attractive (i.e. negative values) and becomes stronger at $d_w \approx 8$ nm. The amount of salt strongly affects the magnitude and the range of this force. As can be seen, for the same σ_M and χ, going from a situation of no added salt to 100 mM NaCl, drastically reduces the electrostatic attraction. While in the absence of added salt, the total potential (V_{total}) is almost entirely attractive, and clearly dominated by the electrostatic potential (even in the presence of the polymer brush), in the presence of 100 mM NaCl, the electrostatic potential reduces significantly to a point where it becomes comparable to the opposing steric repulsion (Fig. 10b). While in Fig. 10a (no added salt) the potential is highly favorable for attachment, in Fig. 10b (100 mM salt) due to the weakened electrostatics by salt, when two liposomes approach each other, they will first feel an energy barrier or peak (which we denote ΔV_1 — Fig. 10b), caused by PEG2K. After passing this peak/barrier the liposomes come to a close separation, which constitutes a minimum in energy (c.f. the energy well in Fig. 10b at ≈3 nm). For the membranes to separate again, they have to overcome the energy barrier ΔV_2. If the energy difference between these two barriers ($\Delta V_{tot} = \Delta V_2 - \Delta V_1$) is negative, or alternatively, if the well at ≈3 nm is lower in energy than the well at ≈14 nm (which means the well at 3 nm is an absolute energy minimum), attachment of liposomes is favored (as long as ΔV_1 is not very high — c.f. Fig. S8 in SI for plots of ΔV_1).

Once the liposomes come to this close distance (in the first well) we consider that the attachment is sticky if ΔV_{tot} is negative. At this point, three different events can occur. (i) the liposomes can detach (not very favorable if ΔV_{tot} is indeed negative,); (ii) the vesicles can fuse; and (iii), one liposome can break, and roll over the intact liposome, coating it and forming a lipid–DNA–lipid sandwich, i.e. forming a lipid–DNA complex. (ii) and (iii) were experimentally observed with cryo-TEM [51]. Hence, if sticky attachment occurs, the probability of complexation to occur is high. We will come back to this.

Coming back to Fig. 10a, as can be seen, even thought PEG2K opposes attachment (hence, complexation), if there is no added salt, the electrostatic force is still high enough (at least at $\chi = 0.9$) to overcome this barrier. On the other hand, in the presence of salt, if PEG2K were not present, the electrostatic force would still be high enough to drive complexation (i.e. the total potential would be equal to the blue line in Fig. 10b). Hence, it becomes clear that it is the combination of both salt (weakens the electrostatics) and PEG2K (opposes attachment), that most effectively prevent liposome attachment, which is indeed what we find experimentally. Lowering χ (which effectively is a reduction in the membrane charge density) also leads to a decrease in the electrostatic attraction, as can be seen when going from Fig. 10b to c. The overall potential for $\chi = 0.4$ is still (barely) favorable to attachment, but only because now the steric repulsion is also lower (mushroom regime). Low σ_M complexes have weakened electrostatics even at low salt, and therefore, the destabilizing effect of polymer is felt at lower amounts of salt.

We have seen that sticky attachment (which ultimately leads to complexation) between liposomes is favored when ΔV_{tot} is negative. ΔV_{tot} becomes less negative at: high salt; high PEG2K%; and also when σ_M and χ become lower. While the amount of salt, PEG2K%, and nominal membrane charge density (σ_M) are well-defined compositional variables; the χ parameter, should be very broad, and, as an approximation, we consider that the states from 0 to 1[3] occur with equal probability. In Fig. 11 the values of ΔV_{tot} are plotted for different values of χ and salt, for the mushroom and brush regimes. In the brush regime, for no added salt, attachment is favored for $\chi \geq 0.5$. For 50 mM salt, attachment is favored for $\chi \geq 0.7$; for 100 mM, for $\chi > 0.8$, and for 150 mM only for $\chi > 0.9$. Hence, the χ interval favorable for sticky attachment is being reduced when C_s and amount of PEG2K are being increased. In the

[3] Again, the situation exactly described by $\chi = 1$ corresponds to that of one liposome completely saturated with DNA to the point that its charge is exactly inversed (e.g. from $+\sigma$ to $-\sigma$), interacting with a DNA-depleted liposome, bearing in mind all the approximations performed this far, this state could also be considered to mimic with some approximation that of a DNA-saturated liposome meeting a naked liposome.

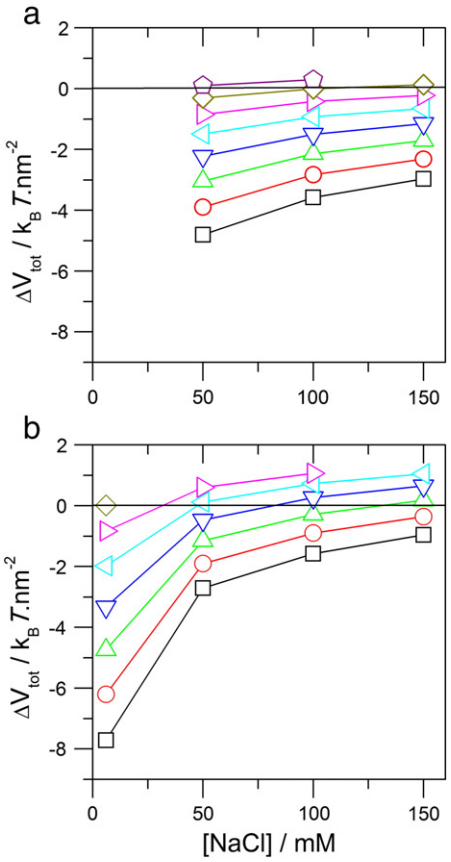

Fig. 11. ΔV_{tot} values for different χ and salt concentrations, and for the mushroom (a) and brush (b) regimes. For a given salt concentration and χ, "sticky" attachment is favored if ΔV_{tot} is negative. Legend: bottom to top: $\chi = 1$; $\chi = 0.9$; $\chi = 0.8$; $\chi = 0.7$; $\chi = 0.6$; $\chi = 0.5$; $\chi = 0.4$; $\chi = 0.3$.

mushroom regime, sticky attachment is favored for a broader range, starting at lower χ, due to the weaker PEG2K repulsion. Because larger χ intervals indicate more reactive liposomes, and because complexation only occurs after DNA-coated liposomes attach, the larger χ intervals at low salt and low PEG2K eventually lead to a higher number of lamellar layers (n_L) in the complexes formed in water when compared to the ones formed in salt. Because complexation involves more drastic rearrangements (i.e. outer liposome breakage and rolling/coating over the inner liposome) and should imply an even greater gain in energy,[4] complex formation is almost irreversible under the studied conditions. I.e. the equilibrium L_α^C state is reached. This is why complexes formed in water, with a large number of layers, remain stable after addition of salt up to 150 mM. Because up to this salt concentration, only the attachment process is significantly affected, once this kinetic barrier is passed, and the complex is formed, complexes remain stable.

As also suggested [51,54], after one outer liposome breaks and rolls over an inner liposome, forming a new lipid–DNA–lipid sandwich (or complex), the monolayer that once was in the inner pool, becomes now exposed to the exterior as the outermost complex layer. This layer has a higher probability of being free of DNA, which would lead to a higher attraction with a DNA-coated liposome. Hence, a freshly formed complex has a higher chance of attaching to another liposome, than two individual (non-complexed) liposomes. This brings some cooperativity to the complexation process and would lead to a nucleation and growth mechanism, controlled by electrostatics (σ_M, χ, C_s, ρ) and steric polymer repulsions (%PEG2K).

The overall conclusions so far are also applicable when analyzing the results of low membrane charge density (σ_M) complexes. In this model, a low σ_M complex is effectively similar to a high σ_M complex with $\chi = 0.6$, and therefore, the number of states χ favoring attachment (and complex formation) is much reduced. In the mushroom regime, with no added salt, attachment is favored for $0.3 \leq \chi \leq 0.6$ ($\approx$30% of the states), and for 150 mM salt, favored for $0.5 \leq \chi \leq 0.6$ ($\approx$10% of the states). The magnitude of this interval is similar to the one from high σ_M complexes with 10% PEG2K (brush regime), and therefore, both states (low σ_M in the mushroom regime and high σ_M in the brush regime) should originate complexes with a similar number of layers.

In the brush regime, the low membrane charge density brings more dramatic effects, as also found experimentally. Now, even in the absence of added salt, only the $\chi = 0.5$ and $\chi = 0.6$ states are favorable for attachment, resulting in a smaller number of layers as compared to the high membrane charge density complexes. In addition, addition of 50 mM of salt drops the electrostatic attraction to values that are already comparable to the steric repulsion in the brush regime, and at 100 mM salt, ΔV_{tot} is already positive at $\chi = 0.6$. Hence, sticky attachment of the liposomes is not favorable for any χ at low σ_M and brush regime above 100 mM salt. The experimental observation that indeed low σ_M complexes with 10% PEG2K do not form at $C_s \geq 100$ mM (excluding the possibility of lipid demixing, as pointed out before) suggests the validity of the overall picture provided with this simple model.

This simple model based on kinetic arguments is also able to explain why complexes with excess CL ($\rho = 3$ and 10) have a larger number of layers when compared to complexes with excess DNA ($\rho = 0.5$). In $\rho = 0.5$ complexes, there is a large excess of DNA, which should lead to a more homogeneous absorption of DNA over the liposomes. This should lead to many liposomes with identical σ_M (i.e. low χ values), leading to weakened electrostatic attraction between liposomes and consequently low number of layers. Conversely, for $\rho = 3$ there is a large excess of "naked" liposomes, which will attract more strongly to DNA-coated liposomes (i.e. high χ values), favoring complexes with a larger number of layers.

5. Conclusions

In this work we have shown that the simple order of mixing (i) cationic liposome, (ii) DNA and (iii) preparation media, has profound effects on the formation structure of PEGylated CL–DNA particles. This behavior is in contrast to that for non-PEGylated complexes, where the order of mixing is less relevant up to 150 mM NaCl. Complexes prepared in water first, and transferred to saline media later, are normally well structured, with a large number of lamellar layers (n_L), and stable with time. This is almost independent of the PEG2K % and membrane charge density (σ_M). Conversely, if complexes are prepared in salt, the number of layers is reduced drastically. This effect is more evident with increasing PEG2K coverage and low σ_M. In the limit of highest coverage studied (10 mol% PEG2K) and lowest σ_M, complexes do not form at physiological ionic strength.

Each of these structures (high and low number of layers) is stable with time, suggesting that despite complex formation being thermodynamically favored, the complexation process in PEGylated membranes, which determines the number of layers per particle, is kinetically controlled.

The results can be explained and modeled by considering a balance of attractive electrostatic forces (favoring CL–DNA formation) and repulsive steric forces caused by PEG2K (opposing CL–DNA formation) that are crucial in the attachment of two partially DNA-coated liposomes (what is most likely the rate-limiting step of PEGylated complex formation). PEG2K opposes the attachment of one DNA-coated liposome to another, but this barrier is overcome by the electrostatic attraction at low salt conditions. If the salinity of the media increases, the

[4] Complexation is also favored by the same factors that favor sticky attachment I.e. electrostatics are still the major force keeping DNA and lipid together, and the polymer is still confined to a small volume. So if ΔV_{tot} is negative (from attachment), the complexation process should also be favored, with a higher energy gain, but proportional to ΔV_{tot}.

electrostatic attraction is reduced, leading to a decrease in the number of layers.

This result is relevant for the gene therapy community, since both the size and number of layers may have implications in the pathways of gene delivery in vitro and in vivo. In addition, it may be useful for the development of lipid–DNA particles with controlled number of layers and/or size.

Acknowledgements

We acknowledge support by NSF DMR-1101900 (phase behavior of lipid/DNA complexes), DOE–BES grant number DE-FG02-06ER46314 (interplay between attractive electrostatic and repulsive polymer forces in lipid/DNA nanoparticle assembly), and NIH GM-59288. BFBS was supported by a Marie Curie International Outgoing Fellowship within the EU Seventh Framework Programme for Research and Technological Development (2007–2013), under grant agreement no. PIOF-GA-2009-252701. CLC thanks Dr. Yeukuang Hwu (Physics Department, Academia Sinica) and Dr. Yen-Ju Chen (NSRRC). UO acknowledges the Swedish Research Council for financial support. CRS acknowledges useful discussions with KAIST Faculty where he has a WCU (World Class University) Visiting Professor of Physics appointment supported by the National Research Foundation of Korea funded by the Ministry of Education, Science and Technology grant No. R33-2008-000-10163-0. This work made use of the Central Facilities of the Materials Research Laboratory at UCSB which is supported by the MRSEC Program of the NSF under award no. DMR-1121053; a member of the NSF-funded Materials Research Facilities Network (www.mrfn.org). The X-ray diffraction work was carried out at the Stanford Synchrotron Radiation Lightsource (SSRL) beam line 4.2.

Appendix A. Supplementary data

The supporting information (SI) includes: additional details on the modeling procedure; the colocalization micrographs for low membrane charge density (σ_M) complexes (Fig. S1); SAXS profiles of high σ_M complexes for $\rho = 0.5$ (Fig. S2); SAXS profiles of low σ_M complexes for $\rho = 3$ and $\rho = 0.5$ (Figs. S3 and S4, respectively); the lamellar *d* spacing for high and low σ_M, and $\rho = 3$ and $\rho = 0.5$, as a function of salt and also DMEM (Fig. S5); SAXS data for PEGylated liposomes alone (no DNA) in water and 150 mM NaCl (Fig. S6); the fitted n_L values for high and low σ_M, at $\rho = 0.5$, as a function of salt and also DMEM (Fig. S7); and plots of ΔV_1 for different χ in the mushroom and brush regimes as a function of C_s (Fig. S8). Supplementary data to this article can be found online at http://dx.doi.org/10.1016/j.bbamem.2013.09.008.

References

[1] Advances in genetics, in: L. Huang, M.-C. Hung, E. Wagner (Eds.), Second ed., Non-Viral Vectors for Gene Therapy, Vol 53, Elsevier, San Diego, 2005.
[2] K.K. Ewert, A. Zidovska, A. Ahmad, N.F. Bouxsein, H.M. Evans, C.S. McAllister, C.E. Samuel, C.R. Safinya, Cationic lipid–nucleic acid complexes for gene delivery and silencing: pathways and mechanisms for plasmid DNA and siRNA, Top. Curr. Chem. 296 (2010) 191–226.
[3] P.L. Felgner, T.R. Gadek, M. Holm, R. Roman, H.W. Chan, M. Wenz, J.P. Northrop, G.M. Ringold, M. Danielsen, Lipofection: a highly efficient, lipid-mediated DNA-transfection procedure, Proc. Natl. Acad. Sci. U. S. A. 84 (1987) 7413–7417.
[4] Z. Rehman, I.S. Zuhorn, D. Hoekstra, How cationic lipids transfer nucleic acids into cells and across cellular membranes: recent advances, J. Control. Release 166 (2013) 46–56.
[5] T. Wang, J.R. Upponi, V.P. Torchilin, Design of multifunctional non-viral gene vectors to overcome physiological barriers: dilemmas and strategies, Int. J. Pharm. 427 (2012) 3–20.
[6] G. Caracciolo, H. Amenitsch, Cationic liposome/DNA complexes: from structure to interactions with cellular membranes, Eur. Biophys. J. 41 (2012) 815–829.
[7] J.O. Rädler, I. Koltover, T. Salditt, C.R. Safinya, Structure of DNA–cationic liposome complexes: DNA intercalation in multilamellar membranes in distinct interhelical packing regimes, Science 275 (1997) 810–814.
[8] D.D. Lasic, H. Strey, M.C.A. Stuart, R. Podgornik, P.M. Frederik, The structure of DNA–liposome complexes, J. Am. Chem. Soc. 119 (1997) 832–833.
[9] I. Koltover, T. Salditt, J.O. Raedler, C.R. Safinya, An inverted hexagonal phase of cationic liposome–DNA complexes related to DNA release and delivery, Science 281 (1998) 78–81.
[10] K.K. Ewert, H.M. Evans, A. Zidovska, N.F. Bouxsein, A. Ahmad, C.R. Safinya, A columnar phase of dendritic lipid-based cationic liposome–DNA complexes for gene delivery: hexagonally ordered cylindrical micelles embedded in a DNA honeycomb lattice, J. Am. Chem. Soc. 128 (2006) 3998–4006.
[11] A. Zidovska, H.M. Evans, K.K. Ewert, J. Quispe, B. Carragher, C.S. Potter, C.R. Safinya, Liquid crystalline phases of dendritic lipid–DNA self-assemblies: lamellar, hexagonal and DNA bundles, J. Phys. Chem. B 113 (2009) 3694–3703.
[12] C. Leal, N.F. Bouxsein, K.K. Ewert, C.R. Safinya, Highly efficient gene silencing activity of siRNA embedded in a nanostructured gyroid cubic lipid matrix, J. Am. Chem. Soc. 132 (2010) 16841–16847.
[13] C. Leal, K.K. Ewert, R.S. Shirazi, N.F. Bouxsein, C.R. Safinya, Nanogyroids incorporating multivalent lipids: enhanced membrane charge density and pore forming ability for gene silencing, Langmuir 27 (2011) 7691–7697.
[14] A. Bilalov, U. Olsson, B. Lindman, A cubic DNA–lipid complex, Soft Matter 5 (2009) 3827–3830.
[15] A. Ahmad, H.M. Evans, K. Ewert, C.X. George, C.E. Samuel, C.R. Safinya, New multivalent cationic lipids reveal bell curve for transfection efficiency versus membrane charge density: lipid–DNA complexes for gene delivery, J. Gene Med. 7 (2005) 739–748.
[16] A. Lin, N. Slack, A. Ahmad, C. George, C. Samuel, C.R. Safinya, Three-dimensional imaging of lipid gene-carriers: membrane charge density controls universal transfection behavior in lamellar cationic liposome–DNA complexes, Biophys. J. 84 (2003) 3307–3316.
[17] S. Golan, B.S. Aytar, J.P.E. Muller, Y. Kondo, D.M. Lynn, N.L. Abbott, Y. Talmon, Influence of biological media on the structure and behavior of ferrocene-containing cationic lipid/DNA complexes used for DNA delivery, Langmuir 27 (2011) 6615–6621.
[18] O. Zelphati, L.S. Uyechi, L.G. Barron, F.C. Szoka Jr., Effect of serum components on the physico-chemical properties of cationic lipid/oligonucleotide complexes and on their interactions with cells, Biochim. Biophys. Acta 1390 (1998) 119–133.
[19] In: D.D. Lasic, F.J. Martin (Eds.), Stealth Liposomes, CRC Press, Boca Raton, 1995.
[20] D.C. Drummond, O. Meyer, K. Hong, D.B. Kirpotin, D. Papahadjopoulos, Optimizing liposomes for delivery of chemotherapeutic agents to solid tumors, Pharmacol. Rev. 51 (1999) 691–743.
[21] L.C. Gomes-da-Silva, N.A. Fonseca, V. Moura, M.C.P. de Lima, S. Simões, J.N. Moreira, Lipid-based nanoparticles for siRNA delivery in cancer therapy: paradigms and challenges, Acc. Chem. Res. 45 (2012) 1163–1171.
[22] T.M. Allen, A. Chonn, Large unilamellar liposomes with low uptake into the reticuloendothelial system, FEBS Lett. 223 (1987) 42–46.
[23] A. Gabizon, D. Papahadjopoulos, Liposome formulations with prolonged circulation time in blood and enhanced uptake in tumors, Proc. Natl. Acad. Sci. U. S. A. 85 (1988) 6949–6953.
[24] A. Gabizon, D.C. Price, J. Huberty, R.S. Bresalier, D. Papahadjopoulos, Effect of liposome composition and other factors on the targeting of liposomes to experimental tumors: biodistribution and imaging studies, Cancer Res. 50 (1990) 6371–6378.
[25] M.C. Woodle, M. Neuman, L.R. Collins, C. Redemann, F.J. Martin, Improved long circulating liposomes "Stealth" using synthetic lipids, Proc. Int. Symp. Control. Release Bioact. Mater. 17 (1990) 77.
[26] A.L. Klibanov, K. Maruyama, V.P. Torchilin, L. Huang, Amphipathic polyethyleneglycols effectively prolong the circulation time of liposomes, FEBS Lett. 268 (1990) 235–237.
[27] G. Blume, G. Cevc, Liposomes for sustained drug release in vivo, Biochim. Biophys. Acta 1029 (1990) 91–97.
[28] T.M. Allen, C. Hansen, F. Martin, C. Redemann, A. Yau-Young, Liposomes containing synthetic lipid derivatives of poly(ethylene glycol) show prolonged circulation half-lives in vivo, Biochim. Biophys. Acta 1066 (1991) 29–36.
[29] D. Papahadjopoulos, T.M. Allen, A. Gabizon, E. Mayhew, K. Matthay, S.K. Huang, K.-D. Lee, M.C. Woodle, D.D. Lasic, C. Redemann, F.J. Martin, Sterically stabilized liposomes: improvements in pharmacokinetics and antitumor therapeutic efficacy, Proc. Natl. Acad. Sci. U. S. A. 88 (1991) 11460–11464.
[30] A. Mori, A.L. Klibanov, V.P. Torchilin, L. Huang, Influence of the steric barrier activity of amphipathic poly(ethyleneglycol) and ganglioside GM1 on the circulation time of liposomes and on the target binding of immunoliposomes in vivo, FEBS Lett. 284 (1991) 263–266.
[31] J. Israelachvili, Intermolecular and Surface Forces with Application to Colloidal and Biological Systems, Academic Press, London, 1985.
[32] A. Martin-Herranz, A. Ahmad, H.M. Evans, K. Ewert, U. Schulze, C.R. Safinya, Surface functionalized cationic lipid–DNA complexes for gene delivery: PEGylated lamellar complexes exhibit distinct DNA–DNA interaction regimes, Biophys. J. 86 (2004) 1160–1168.
[33] H. Hatakeyama, H. Akita, H. Harashima, A multifunctional envelope type nano device (MEND) for gene delivery to tumours based on the EPR effect: a strategy for overcoming the PEG dilemma, Adv. Drug Deliv. Rev. 63 (2011) 152–160.
[34] I. MacLachlan, P. Cullis, Diffusible-PEG-lipid stabilized plasmid lipid particles, Adv. Genet. 53PA (2005) 157–188.
[35] B. Romberg, W.E. Hennink, G. Storm, Sheddable coatings for long-circulating nanoparticles, Pharm. Res. 25 (2008) 55–71.
[36] C.-L. Chan, R.N. Majzoub, R.S. Shirazi, K.K. Ewert, Y.-J. Chen, K.S. Liang, C.R. Safinya, Endosomal escape and transfection efficiency of PEGylated cationic liposome–DNA complexes prepared with an acid-labile PEG-lipid, Biomaterials 33 (2012) 4928–4935.
[37] G. Basha, T.I. Novobrantseva, N. Rosin, Y.Y.C. Tam, I.M. Hafez, M.K. Wong, T. Sugo, V.M. Ruda, J. Qin, B. Klebanov, M. Ciufolini, A. Akinc, Y.K. Tam, M.J. Hope, P.R. Cullis,

Influence of cationic lipid composition on gene silencing properties of lipid nanoparticle formulations of siRNA in antigen-presenting cells, Mol. Ther. 19 (2011) 2186–2200.
[38] Y. Nie, D. Schaffert, W. Rodl, M. Ogris, E. Wagner, M. Gunther, Dual-targeted polyplexes: one step towards a synthetic virus for cancer gene therapy, J. Control. Release 152 (2011) 127–134.
[39] P.L. DeHaseth, T.M. Lohman, M.T. Record Jr., Nonspecific interaction of lac repressor with DNA: an association reaction driven by counterion release, Biochemistry 16 (1977) 4783–4790.
[40] R. Bruinsma, Electrostatics of DNA–cationic lipid complexes: isoelectric instability, Eur. Phys. J. B 4 (1998) 75–88.
[41] D. Harries, S. May, W.M. Gelbart, A. Ben-Shaul, Structure, stability, and thermodynamics of lamellar DNA–lipid complexes, Biophys. J. 75 (1998) 159–173.
[42] I. Koltover, T. Salditt, C.R. Safinya, Phase diagram, stability, and overcharging of lamellar cationic lipid–DNA self-assembled complexes, Biophys. J. 77 (1999) 915–924.
[43] Lipofectamine®, Reagent, http://tools.invitrogen.com/content/sfs/manuals/lipofectamine2000_man.pdf2000.
[44] A. Caillé, X-ray scattering by smectic-A crystals, C. R. Acad. Sci. Ser. B 274 (1972) 891.
[45] C.R. Safinya, D. Roux, G.S. Smith, S.K. Sinha, P. Dimon, N.A. Clark, A.M. Bellock, Steric interactions in a model multimembrane system: a synchrotron X-ray study, Phys. Rev. Lett. 57 (1986) 2718–2721.
[46] J. Als-Nielsen, J.D. Litster, R.J. Birgeneau, M. Kaplan, C.R. Safinya, A. Lindegaard-Andersen, S. Mathiesen, Observation of algebraic decay of positional order in a smectic liquid crystal, Phys. Rev. B 22 (1980) 312–320.
[47] C.R. Safinya, E.B. Sirota, R.J. Plano, Nematic to smectic-A phase transition under shear flow: a nonequilibrium synchrotron X-ray study, Phys. Rev. Lett. 66 (1991) 1986–1989.
[48] N.F. Bouxsein, C. Leal, C.S. McAllister, K.K. Ewert, Y. Li, C.E. Samuel, C.R. Safinya, Two-dimensional packing of short DNA with nonpairing overhangs in cationic liposome–DNA complexes: from Onsager nematics to columnar nematics with finite-length columns, J. Am. Chem. Soc. 133 (2011) 7585–7595.
[49] L.D. Landau, Collected Papers of L D Landau, in: D. Ter Haar (Ed.), Intl Pub Distributor Inc, 1965, p. 209.
[50] R.E. Peierls, Remarks on transition temperatures, Helv. Phys. Acta 7 (Suppl. 2) (1934) 81.
[51] S. Huebner, B.J. Battersby, R. Grimm, G. Cevc, Lipid–DNA complex formation: reorganization and rupture of lipid vesicles in the presence of DNA as observed by cryoelectron microscopy, Biophys. J. 76 (1999) 3158–3166.
[52] S. Weisman, D. Hirsch-Lerner, Y. Barenholz, Y. Talmon, Nanostructure of cationic lipid–oligonucleotide complexes, Biophys. J. 87 (2004) 609–614.
[53] D. Merkle, S.P. Lees-Miller, D.T. Cramb, Structure and dynamics of lipoplex formation examined using two-photon fluorescence cross-correlation spectroscopy, Biochemistry 43 (2004) 7263–7272.
[54] E.V. Pozharski, R.C. MacDonald, Single lipoplex study of cationic lipid–DNA, self-assembled complexes, Mol. Pharm. 4 (2007) 962–974.
[55] A.A. Meier-Koll, C.C. Fleck, H.H. von Grünberg, The counterion–release interaction, J. Phys. Condens. Matter 16 (2004) 6041–6052.
[56] M. Silvander, Steric stabilization of liposomes — a review, Progr. Colloid. Polym. Sci. 120 (2002) 35–40.